

Reaction Chemistry & Engineering

Accepted Manuscript



This article can be cited before page numbers have been issued, to do this please use: M. D. Zhurka, A. Lemonidou, J. A. Anderson and P. Kechagiopoulos, *React. Chem. Eng.*, 2018, DOI: 10.1039/C8RE00145F.



This is an Accepted Manuscript, which has been through the Royal Society of Chemistry peer review process and has been accepted for publication.

Accepted Manuscripts are published online shortly after acceptance, before technical editing, formatting and proof reading. Using this free service, authors can make their results available to the community, in citable form, before we publish the edited article. We will replace this Accepted Manuscript with the edited and formatted Advance Article as soon as it is available.

You can find more information about Accepted Manuscripts in the [author guidelines](#).

Please note that technical editing may introduce minor changes to the text and/or graphics, which may alter content. The journal's standard [Terms & Conditions](#) and the ethical guidelines, outlined in our [author and reviewer resource centre](#), still apply. In no event shall the Royal Society of Chemistry be held responsible for any errors or omissions in this Accepted Manuscript or any consequences arising from the use of any information it contains.

Kinetic analysis of the steam reforming of ethanol over Ni/SiO₂ for the elucidation of metal dominated reaction pathways

Marinela D. Zhurka,¹ Angeliki A. Lemonidou,² James A. Anderson,¹ Panagiotis N. Kechagiopoulos^{1*}

¹Chemical and Materials Engineering Group, School of Engineering, University of Aberdeen, Aberdeen, AB24 3UE, UK

²Laboratory of Petrochemical Technology, Department of Chemical Engineering, Aristotle University of Thessaloniki, GR-54124 Thessaloniki, Greece

* Corresponding author: p.kechagiopoulos@abdn.ac.uk

Abstract

Hydrogen production via steam reforming of biomass derived ethanol is a promising environmental alternative to the use of fossil fuels and a means of clean power generation. A kinetic study of ethanol steam reforming (ESR) is presented, where the effect of temperature, space time and partial pressure of reactants is investigated over a wide range in a fixed bed reactor over a Ni/SiO₂ catalyst. The order of the reaction was found to be 0.5 in ethanol and almost zero in water, indicating a steam-independent rate limiting step, while an apparent activation energy of 48 kJ mol⁻¹ was obtained. Identification of primary and secondary products revealed the reaction mechanism to be strongly affected by temperature with results suggesting the existence of two alternate pathways being active, one involving acetaldehyde and one an ethanol decomposition derived surface intermediate. Below 450°C ethanol decomposition and dehydrogenation were found to be dominant, whereas at higher temperatures secondary methane steam reforming (MSR) and water-gas shift (WGS) reactions became enhanced. Excess of water was able to promote the WGS and suppress the methanation reaction even at 400°C. Time-on-stream studies at 500°C revealed Ni/SiO₂ to have a good balance between stability, activity and selectivity in ESR. Temperature programmed oxidation (TPO) and hydrogenation (TPH) analyses indicated that the carbonaceous deposits were graphitic in nature, suggesting the presence of filamentous coke.

Keywords: Ethanol steam reforming; Nickel, Silica support, Kinetic study

1. Introduction

The rapid increase in society's industrialization has led to a significant rise in energy consumption demands, which are currently predominantly satisfied from fossil fuels. The foreseen depletion of the latter and the environmental issues with emissions due to their extensive use, have intensified research on alternative, renewable, energy sources. Hydrogen is a clean energy carrier that, when derived from renewable sources can be used for the sustainable production of electricity (via fuel cells) and/or heat.¹ Currently it is mainly produced from non-renewable sources, such as natural gas, leading to high CO₂ emissions. A promising sustainable route for hydrogen production is ethanol steam reforming (ESR), which has attracted considerable research interest.² It can be produced from various renewable sources, such as energy crops, forestry or agro-industry waste, the organic fraction of municipal solid waste, etc. via hydrolysis and fermentation processes.³ It has low toxicity and, being a liquid, it presents advantages related to ease of transportation and storage. Ethanol can also be regarded as a model compound of the carbohydrate-derived fraction of bio-oil, the liquid product of biomass pyrolysis. Steam reforming of the latter has also been proposed as a promising route for sustainable hydrogen production,⁴⁻⁶ hence studies of ESR can further contribute to the understanding of that process.

ESR proceeds according to the overall stoichiometry of reaction (1) shown in Table 1. The water-gas shift reaction (2) that occurs in parallel further influences hydrogen production and the respective ratio of carbon oxides observed in the products. Nonetheless, a range of additional products have also been reported in literature, namely methane, acetaldehyde, ethylene, and acetic acid participating in reactions (3) to (10), while less frequently even acetone has been observed.⁷ Among several available kinetic investigations on Ni, the reaction order has been mainly reported as positive for ethanol⁸⁻¹¹ and negative^{12,13} for water, the latter fact pointing to the competitive adsorption of ethanol and water on the same site. A range of apparent activation energy values from about 32 kJ

mol⁻¹ to 90 kJ mol⁻¹ have also been reported^{7,8,14,15} indicative of the large effect of catalyst properties and/or operating conditions on the parameter.

The reaction mechanism of ESR has also been the subject of several experimental and theoretical studies.^{13,16–18} Sanchez et al.¹⁹ investigated ESR on Pt, Ni and PtNi catalysts supported on γ -Al₂O₃, suggesting the main reaction pathway to be that of ethanol dehydrogenation followed by the decomposition of acetaldehyde or the oxidation of the latter towards surface acetate species. Sutton et al.²⁰ developed a comprehensive microkinetic model for ESR over Pt based on elaborate DFT calculations, exploring oxidative dehydrogenation reactions as possible alternatives to pure decomposition ones. The main pathway was found to be determined by the decomposition of ethanol, followed by the water-gas shift reaction. Wang et al.¹⁵ presented a Langmuir-Hinshelwood kinetic analysis of ESR over an Ir/CeO₂ catalyst based on a bi-functional mechanism, where adsorption of ethanol and formation of ethoxy and acetaldehyde occur on the support, while CO and H₂ formation takes place on the metal.

The formation of coke and its type have also been the focus of different studies,^{21–23} with the Boudouard reaction (11), the decomposition of methane (12) and the polymerization of ethylene (13) highlighted as the main pathways to carbon deposition. Noble metals catalysts have typically shown high activity with negligible coke formation,^{24,25} however their high cost has led to the extensive investigation of non-noble metal catalysts as well. Ni has been widely studied and proven to be most active for ESR, although carbon deposition remains a major challenge. In this regard, appropriate operating conditions, such as high temperature and steam to carbon ratio, can decrease the production of coke or lead to filamentous deposits that do not impact severely on activity. Moreover, coking has been linked with the nature of the support²³ and, specifically, the formation of ethylene over acidic sites via the dehydration of ethanol, hence basic supports are preferred.

The current work aims to establish the metal dominated reaction pathways of ESR over Ni. For this purpose, SiO₂, being relatively inert, non-reducible and with low acidity, is selected as a suitable

catalyst support. Ni/SiO₂ catalysts have been studied already for ESR, however most work to date has focused either on catalytic activity and coke formation^{26,27} or on the investigation of different catalyst preparation methods.^{28,29} The reaction pathways of ESR have also been investigated on Ni/SiO₂, although using a fluidised bed and obtaining overall relatively high conversions, while focus was primarily on coke formation mechanisms.²¹ In the current work a complete kinetic study of ESR is presented over a wide range of experimental conditions in a fixed bed reactor, aiming at the elucidation of the reaction mechanism and the identification of primary and secondary products. The metal dominated kinetic data collected further provide base-line activity for Ni, so that support effects can be considered and (micro-) kinetic models can be developed describing these interactions.

2. Experimental procedures

2.1. *Sample preparation*

Nickel silica catalysts with nominal 10wt. % Ni were prepared using Ni(NO₃)₂·6H₂O as precursor and Aerosil 200 (surface area 179 m² g⁻¹) as support. An aqueous solution of nickel nitrate was added to a suspension of silica at room temperature with constant stirring before raising the temperature to 353 K to slowly remove water. The sample was then placed in an oven overnight at 363 K with regular mixing and grinding to ensure homogeneity while removing final traces of moisture. The dried sample was then calcined at 673 K in a flow (50 cm³ min⁻¹) of air for 2 h and then subsequently reduced at the same temperature in a flow (50 cm³ min⁻¹) of hydrogen for 2 h. The resultant sample gave a hydrogen uptake at 298 K of 165 μmoles g⁻¹ which equated to a dispersion of 38.6 %.

2.2. *Reactor setup*

The kinetic study took place in a fully automated reaction system by PID Eng & Tech (Micro Activity-Effi unit). An HPLC pump (Gilson 307) was used to deliver the ethanol/water feed. The latter was channelled at appropriate residence time through the hot box of the unit, operating at 150°C, to

ensure evaporation. The vapours were subsequently mixed with N₂, fed via a mass flow controller (Bronkhorst El-Flow Select), the former also used as an internal standard during gas products analysis via GC. Reaction products upon exiting the hot box were fed into a Gas/Liquid separator, operated at 0°C, where condensables were separated and collected. Analysis of the gas products took place on-line via a HP5890 GC equipped with a TCD detector and MS-5A and HS-T columns, while liquids were analysed off-line in a Thermo Scientific TRACE 1300 GC equipped with an FID detector and a TG WAXMS A column.

A stainless steel (SS316) fixed bed reactor (9.1 mm i.d. and total length 304.8 mm) was used for all kinetic experiments, heated by a single-zone furnace, able to provide an isothermal region of 5 cm. The internal surface of the reactor was passivated with an alumina-based layer to minimize catalytic effects, while a fitted porous plate (Hastelloy C) ensured that the catalyst bed remained in the furnace's isothermal zone. A thermocouple inside the reactor in a fixed position of 5 mm above the porous plate was used for temperature measurement and control. The catalyst was deposited above a thin layer of α -Al₂O₃ (1.5 mm), which was also used as diluent, while quartz wool was placed at both ends to support the bed in the tube.

2.3. *Experimental conditions and parameters*

Before each experiment the catalyst was reduced at 500°C using a flow of 5 % H₂ on N₂ for 1 h. TPR profiles and XRD patterns of the fresh catalyst evidenced the full reduction of NiO to Ni. Reaction temperature was varied over a range of 300-600°C at an inlet molar Steam/Carbon (S/C) ratio of 3. The effect of partial pressure of ethanol was studied varying the latter from 0.03 to 0.18 bar at 400°C, keeping the partial pressure of water constant at 0.35 bar. Similarly, the effect of partial pressure of water was studied over a range of 0.12 to 0.74 bar at 400°C, at a constant partial pressure of ethanol of 0.06 bar. In both cases, these ranges were equivalent to a S/C variation of 1 to 6, while a N₂ flow was used to maintain an overall constant volumetric flow rate. The space time effect was studied at two different reaction temperatures of 400 and 550°C at a S/C ratio of 3,

varying the ratio of the catalyst mass over the mass flow rate of ethanol, $W/F_{\text{Eth},t0}$, from 58.2 to 349.4 $\text{g}_{\text{cat}} \text{ s g}_{\text{Eth}}^{-1}$, by changing the ethanol and water feed over a fixed mass of catalyst and flow of N_2 resulting in variation of the total volumetric rate from 330 to 97 $\text{cm}^3 \text{ min}^{-1}$ (STP). Stability runs were carried out in the same reaction system at a temperature of 500°C and S/C of 3, at a space time of 358.7 $\text{g}_{\text{cat}} \text{ s g}_{\text{Eth}}^{-1}$ and total volumetric rate of 98 $\text{cm}^3 \text{ min}^{-1}$ (STP). A mass of 80 mg Ni/SiO₂ catalyst was used in all experiments besides the space time run at 550°C, where, due to the higher activity of the catalyst, 26.7 mg were used to maintain ethanol conversion sufficiently low.

Standard criteria by Mears³⁰ and Weisz-Prater³¹ were applied to ensure measurements were conducted under explicit kinetic control and were unaffected by transport limitations. Multiple tests were carried out at the same conditions to verify the repeatability of results, while at the start and end of every experimental session the performance of the catalyst was evaluated at reference conditions (temperature of 400°C and S/C of 3) to ensure deactivation had not occurred. Atomic C, H and O mass balance closure in all tests was in the order of $100 \pm 5 \%$. The results presented in following sections are expressed in terms of the following parameters:

$$\text{Conversion: } X = \frac{\text{moles of carbon converted to products}}{\text{moles of carbon in feed}} \times 100$$

$$\text{Selectivity of } y \text{ compound: } S_c(y) = \frac{\text{moles of carbon converted to } y \text{ compound}}{\text{moles of carbon in feed converted to products}} \times 100$$

$$\text{Hydrogen yield: } Y_{\text{H}_2} = \frac{\text{moles of hydrogen produced}}{6 \times \text{moles of ethanol in the feed}} \times 100$$

Results are further compared with thermodynamic equilibrium at equivalent conditions, calculated via Gibb's free energy minimisation within the Aspen Plus software using the Peng-Robinson equation of state. In line with the reactions appearing in Table 1, compounds considered were ethanol, water, carbon monoxide, methane, carbon dioxide, acetic acid, acetone, acetaldehyde and hydrogen.

2.4. Characterisation of spent catalysts

Temperature Programmed Oxidation (TPO) and Hydrogenation (TPH) analyses were performed by means of an automated gas flow system using a U-tube reactor connected online with a quadrupole mass analyser (OmniStar), as described in detail elsewhere.³² In all TP experiments, spent catalyst samples were pre-treated in a He flow at 250°C for 30 min and then allowed to cool to room temperature. The temperature was subsequently increased to 800°C at a rate of 10°C min⁻¹ under a flow of 30 cm³ min⁻¹ (20 % O₂ in He for TPO and 20 % H₂ in He for TPH). All relevant (*m/z*) mass numbers were monitored via MS to quantify the oxidation or hydrogenation products.³³ On selected spent catalyst samples, carbon deposits were also examined on a C, H elementary analyser (LECO 628) to verify the TPO measurements.

3. Results and Discussion

3.1. Effect of temperature

Figure 1 shows the effect of temperature on the conversion of ethanol and the yield of hydrogen, while in Figure 2 the selectivities towards all carbon containing compounds in comparison with thermodynamic equilibrium are presented. An increase in temperature from 300 to 600°C led to a rise in ethanol conversion from 5 % to almost 70 %, while the equilibrium predicted value was 100 % over the entire range studied. H₂ yield closely followed the trend of conversion, increasing gradually from almost 0 % to 40 %, but remained far from the equilibrium predicted values. The gas product mixture consisted of CO, CO₂, H₂ and CH₄ for all temperatures studied, while CH₃CHO was the most significant liquid product detected, particularly below 450°C. No C₂H₄ was identified in the gas products, a fact most probably linked to the low acidity of the SiO₂ support that disfavours the ethanol dehydration reaction.²¹ Traces of acetic acid (not quantified) were detected in the liquid samples of experiments conducted at low temperatures.

Based on the presented selectivities, two relatively distinct kinetic regimes can be identified in terms of temperature. The overall very low H_2 yield and high CH_3CHO , CH_4 and CO selectivities observed below $450^\circ C$ are evidence that the ethanol dehydrogenation (3) and decomposition (4) reactions dominate over ethanol reforming (1) and water-gas shift (2) in that range. CH_3CHO formed by the dehydrogenation of adsorbed ethanol is considered as a key intermediate in the reaction mechanism of ESR and its existence has been reported in a number of studies.^{14,34,35} The very similar selectivities of CH_4 and CO at $300^\circ C$ is further evidence of the decomposition of CH_3CHO to CH_4 and CO according to reaction (5) or the direct decomposition of ethanol (4) at low temperatures. Below $450^\circ C$, the opposing trends of CH_4 and CO selectivities as temperature rises in combination with the low H_2 yield indicate the occurrence of the methanation reaction (reverse of (6)) and the overall very low activity of the catalyst in the water-gas shift reaction. Given the low activity of the latter reaction, the relatively high CO_2 selectivity, already from the lowest temperatures, is tentatively linked with the formation of acetate species that can further decompose, leading eventually to the formation of CH_4 and CO_2 .³⁶ Acetate species have been detected in FTIR studies during ethanol reforming or decomposition and are thought to be formed through the oxidation of adsorbed CH_3CHO via OH groups.^{19,37} Alternatively, acetate groups may be derived from the adsorption and subsequent reaction of acetic acid or acetone.³⁸ Traces of acetic acid detected at low temperatures in this work further support this, in line with reports³⁹ that suggest the formation of acetic acid from CH_3CHO and steam (reaction (9)) and its further decomposition to CH_4 and CO_2 (reaction (10)).

Above $450^\circ C$, a clear drop in CH_4 selectivity is observed that can be attributed to the increasing activity of the Ni catalyst in the CH_4 steam reforming reaction (6). Above this temperature, the water-gas shift reaction is also promoted, as CO selectivity is seen to decrease, with CO_2 selectivity and H_2 yield concurrently increasing. In fact, evaluating the experimental CO/CO_2 ratio across the entire temperature range suggests that the reaction approaches equilibrium at $500^\circ C$ and above with the experimental ratio of about 0.2-0.5 being close to the equilibrium value. At lower temperatures, the water-gas shift reaction is highly non-equilibrated towards the CO side, with

CO/CO₂ ratios averaging at 1-2 when equilibrium predicts essentially only CO₂ in the product mixture. The CH₃CHO selectivity also approaches zero in the high temperature range further providing evidence that reforming reactions are promoted under these conditions. Overall, the temperature scan showed that below 450°C, both primary ethanol decomposition and dehydrogenation reactions and secondary reactions involving the products of the former were under a clear kinetic regime, with primary ones having a moderate activity and secondary ones being less significant. At higher temperatures, these secondary reactions were clearly enhanced, with the water-gas shift reaction seen to approach equilibrium.

The measurements from 300 to 400°C, having a low conversion of ethanol (<20%), were further used to calculate an apparent activation energy of ESR. Figure 3 presents the Arrhenius plot for this range, based on which an activation energy of 48 kJ mol⁻¹ was calculated. This value is in good agreement with literature, however as discussed also in the Introduction a relatively wide variability in the reported values does exist due to different conditions used, conversions achieved, partial pressures of reactants, etc. Indicatively, using the higher temperature data a value of 32 kJ mol⁻¹ was obtained (Arrhenius plot not shown). The much higher conversions achieved in this range need to be carefully considered when evaluating this value, however its difference from the low temperature one does support the existence of two different kinetic regimes, as discussed above.

3.2. *Effect of partial pressure of reactants*

3.2.1. Variation of ethanol partial pressure

Figure 4a presents the effect of ethanol partial pressure on ethanol conversion and H₂ yield. These experiments were carried out at constant partial pressure of water, overall pressure, and total volumetric flow, using N₂ as balance. A decrease of ethanol partial pressure under these conditions corresponded to an increase of the inlet S/C ratio from 1 to 6. The plot is presented in terms of S/C variation to facilitate further discussion on selectivity trends, however the equivalent partial pressures of ethanol are also annotated. Both ethanol conversion and H₂ yield increased almost

linearly with the S/C ratio (Figure 4a), directly linked to the decreasing flow of ethanol at a constant overall space time used to vary the partial pressure of ethanol. Nonetheless, in Figure 4b the turnover frequency (TOF) is presented as a function of the square route of the partial pressure of ethanol, where the very good linear trend indicates a positive and approximately 0.5 order rate of ESR with respect to ethanol. Results are consistent with previous studies over Pt²⁰ and Ru⁴⁰ and also in the case of Ni^{8,9} that an ethanol derived surface intermediate participates in the rate determining step of ESR. Furthermore, similar partial orders in ethanol, namely 0.43 on Ni¹⁸ and 0.5 on Pt⁴¹, and the associated active site requirements, have served as an indication to suggest either the dissociative adsorption of ethanol or its dissociation on the surface as the most probable rate determining steps.

Figure 5 presents the selectivities of carbon containing products in comparison with equilibrium for these experiments again in terms of S/C ratio with the equivalent partial pressures of ethanol annotated. The decrease in CH₃CHO complies with the suggested primary nature of the species, with its formation linked directly to the rate of ethanol conversion, the latter decreasing with the decrease in ethanol partial pressure (increase in S/C). Considering further the results reported in Section 3.1, where it was seen that at 400°C, the water-gas shift activity was very low, the obvious increase of the CO₂ selectivity versus that of CO with increasing S/C needs to be noted, evidencing the promotion of this reaction under these conditions. Moreover, at this temperature, the participation of the methanation reaction was identified as possible, which the increasing S/C ratio appears to be inhibiting as indicated by the gradual decrease in CH₄ selectivity. In these experiments, the partial pressure of water was held constant, while that of ethanol was varied. Only at S/C = 1 (highest ethanol partial pressure studied), is the water fed sub-stoichiometric for ESR, so evidently the increasing relative abundance of surface hydroxyl groups originating from the dissociation of water in comparison to the ethanol derived intermediates appears to be able to affect the activity of both of these secondary reactions even at the low temperature of 400°C.⁴²⁻⁴⁴ The promoting effect of steam drives the water-gas shift reaction closer to equilibrium as the S/C is increased, although

even at the highest value studied, the experimental CO/CO₂ ratio at 0.4 is markedly higher than the thermodynamically predicted value of 0.02.

3.2.2. Variation of water partial pressure

The effect of partial pressure of water on ethanol conversion and H₂ yield is presented in Figure 6a. These experiments were carried out at constant ethanol partial pressure, overall pressure and total volumetric flow, varying the partial pressure of water and using N₂ as balance. In this case, the increase of water partial pressure has a direct equivalence to the S/C ratio, which again ranges from 1 to 6, nonetheless all relevant plots are, as above, annotated with both parameters. Ethanol conversion at these conditions shows a slightly negative trend with increasing water partial pressure (and S/C) in contrast to what was observed when ethanol partial pressure was varied. This is further evident by the TOF achieved during these experiments (Figure 6b), where a slightly negative, but close to zero, order with respect to the water partial pressure is calculated, with the overall rate of ESR decreasing by a factor of 0.07. The approximately zero order with respect to water indicates that either steam derived surface intermediates do not participate in the rate determining step of ESR or that the surface of the catalyst is already fully covered with such species in the entire range of water partial pressures investigated leading to an overall apparent zero order. The former of the two possibilities is suggested as more probable, considering that a steam-independent kinetic behaviour has been previously discussed both for the steam reforming of methane over Ni catalysts^{45,46} and ESR over other metals.^{20,41,47} Consistent with these works, the slightly negative slope observed is an indication of the competitive adsorption of ethanol and water for the same catalyst active site.⁴⁸

Figure 7 shows the carbon selectivities in comparison to equilibrium for the partial pressure of water variation experiments. It is noteworthy that even though ethanol conversion displays the opposite trend when compared to data in Figure 4, the selectivity trends for all products are the same as those presented in Figure 5. The results are consistent with a reaction mechanism where the rate determining step involves only the decomposition of adsorbed ethanol, while the surface reactions

that involve the further conversion of the decomposition products occur after the rate controlling step. Steam and its dissociation derived surface intermediates, namely hydroxyl and oxygen species, participate in the conversion of the ethanol decomposition fragments, specifically via the water-gas shift and steam reforming reactions. The rising CO_2 selectivity concurrently with the decrease of CO suggest that the excess water on the catalyst surface favours the water-gas shift activity. Considering the low temperature in these experiments the decreasing CH_4 selectivity is linked to the inhibition of the methanation reaction, however at higher temperatures a promotion of the methane steam reforming would be expected, as also seen in Section 3.1. The partial pressure of water in these experiments was specifically varied from 0.18 to 0.74 bar, the latter value being twice that used in the ethanol partial pressure variation experiments, explaining the comparatively lower CO and CH_4 selectivities and the higher CO_2 selectivity obtained. This is further supported by the experimental CO/ CO_2 ratio of 0.19 calculated at the highest water partial pressure, which, in this case, is approximating more the thermodynamically predicted of 0.02 indicating the closer approach to partial-equilibration for the water-gas shift under these conditions. Finally, the selectivity of CH_3CHO is again found to decrease with water partial pressure (and S/C), which is further linked to the reduced rate of ethanol conversion. As discussed in detail in the following section, CH_3CHO is a primary product of ethanol dehydrogenation and its formation should not be affected by steam derived species. In these experiments, the partial pressure and contact time of ethanol were held constant, however, the gradual saturation of the catalyst surface by H_2O led to a drop in the ethanol conversion rate and, as such, to a decrease in the production rate of CH_3CHO . Excess of water has been even suggested to promote the acetaldehyde steam reforming reaction at low temperatures over Ni based catalysts,^{49, 50} so the possibility of such alternate routes being enhanced at the higher water partial pressures cannot be excluded. In all cases, the abundance of H_2O was responsible for the consecutive conversion of the decomposition products of both CH_3CHO and ethanol. Given the trend in CH_3CHO selectivity decreasing at opposing ethanol conversion trajectories during the two partial pressure variation experiments, it is further suggested, tentatively at this stage, that the

primary conversion of ethanol proceeds through surface intermediates that do not involve adsorbed CH_3CHO . More evidence in support of this is provided in the following section.

3.3. *Effect of space time*

3.3.1. Ethanol steam reforming

Figure 8a presents the effect of space time on the conversion of ethanol and H_2 yield obtained at 400°C and 550°C during ethanol steam reforming. In both cases, ethanol conversion increased steadily with space time, while the equilibrium predicted value is 100% for both temperatures. H_2 yield, consistent with results presented in previous sections, is linked directly with the conversion of ethanol and, similarly, increased with W/F. Both conversion and H_2 yield are, as expected, enhanced considerably at the higher temperature, with conversion particularly being almost complete at the largest space time tested at 550°C . Nonetheless, in both temperatures conversion values below 20% were obtained at the lowest W/F to allow the reaction pathway analysis.

The effect of space time on selectivities was specifically used to distinguish primary and secondary products of ESR. The concentration of primary products approaches a finite value as contact time tends to zero, while that of secondary products reaches a zero value.⁵¹ The panels (b) and (c) of Figure 8 present the carbon selectivities of all products for the two studied temperatures in terms of the conversion observed during space time variation. At 400°C the selectivities of CO , CH_4 and CO_2 clearly increase with the increase in conversion, while that of CH_3CHO shows the opposite trend and eventually reaches a value of almost zero at the highest conversions (Figure 8b). More importantly, when looking at the slopes of the selectivity curves for CO , CH_4 and CO_2 it can be seen that, if extrapolated towards zero conversion, they all tend towards the origin. On the contrary, CH_3CHO is the only carbon containing product whose selectivity curve clearly approaches a finite value, which would logically be 100 % if it was possible to carry out experiments at such short contact times. The results underline the primary nature of product CH_3CHO , derived from ethanol dehydrogenation, and the secondary character of CO , CH_4 and CO_2 products originating from decomposition, reforming

and the water-gas shift reactions. The experimental CO/CO₂ ratio decreases from 2.2 to 1.4 as the contact time increases, whereas the thermodynamic value of the ratio at these conditions approaches zero. This is a clear indication that, even though the reaction is tending towards equilibrium, it is still quite far from it at this low operating temperature.

At 550°C the selectivity trends are markedly different to those obtained at the lower temperature (Figure 8c). CH₃CHO selectivity is considerably reduced, consistent with the higher operating temperature promoting further conversion, however, again, the slope can be seen to tend towards a finite value at zero contact times, consistent with the product's primary nature. It is important to note again that, even though the activity was much higher at this temperature, low conversion experiments were carried out to ensure the validity of kinetic information obtained. In the case of CO and CH₄, the selectivities display a clear shift in their trends versus conversion in comparison to 400 °C, with their slopes now also reaching a finite value as they are extrapolated towards zero contact time. Results indicate that both CO and CH₄ are now primary products and suggest that they originate from a species that at 550°C is highly reactive. These trends support the findings of the previous section, where it was suggested that the main pathway of ethanol conversion may not necessarily involve CH₃CHO. Ethanol in part becomes dehydrogenated towards CH₃CHO, which further decomposes to CO and CH₄ or desorbs. However, a parallel surface pathway that accounts for part of the ethanol consumption and involves an intermediate not related to CH₃CHO appears also to be taking place. At 400°C the reaction rate of this path is slow, hence both CO and CH₄ appear as secondary products. At 550°C the same path becomes significant and CO and CH₄ become primary products. Moreover, given the slightly negative kinetic order of steam, this major ethanol conversion pathway must involve the decomposition of ethanol and not its reaction with any steam derived intermediates. Indeed, in a DFT-based microkinetic study²⁰ over Pt, ethanol decomposition primarily takes place via the formation of 1-hydroxyethyl, the latter successively dehydrogenating to 1-hydroxyethylidene and acetyl intermediates. C-C bond scission was found to take place at late stages, mainly at the ketenyl intermediate, formed itself from progressive dehydrogenations of

acetyl species. Current results suggest that a similar pathway could be active over Ni catalysts. CH_3CHO in all cases is directly formed via adsorbed ethanol, from the dehydrogenation of either ethoxy or 1-hydroxyethylidene, hence always behaves as a primary product. CO_2 , finally, is the only carbon-containing product that remains a secondary product at 550°C , highlighting that its major formation pathway involves the water-gas shift reaction and, potentially, methane steam reforming at this high temperature, requiring the intermediate production of CO or CH_4 , respectively. Throughout the space time range studied the CO/CO_2 ratio is much closer to the thermodynamic predicted value, suggesting the reaction approached partial-equilibrium, in line with the results presented in Section 3.1. At short contact times at 550°C , primary decomposition and dehydrogenation reactions of ethanol are significant giving rise to CH_3CHO , CO , CH_4 and H_2 as products. As the contact time increases, CH_3CHO , CO and CH_4 selectivities decrease whilst simultaneously CO_2 selectivity increases since secondary acetaldehyde decomposition, methane steam reforming and water-gas shift reactions are favoured.

3.3.2. Ethanol decomposition

Ethanol decomposition (EDC) at $S/C = 0$ was also investigated to further provide insight into the main reaction pathways. Figure 9a presents the effect of space time on the conversion of ethanol and H_2 yield at 400°C , where again, a gradual increase of both parameters is observed with contact time. However, clearly both conversion and yield are much lower in comparison to the ESR case at equivalent conditions, indicative of the role of steam at promoting the overall conversion through the secondary conversion of primary decomposition products via the water-gas shift and reforming reactions. A maximum conversion of only about 15 % and a H_2 yield below 5 % is achieved at the highest space time tested, whereas under the same conditions during ESR these values were 50 and 30 %, respectively. The very low production of H_2 , in particular, suggests that it only originates from the ethanol dehydrogenation to acetaldehyde and, potentially, the decomposition of methane (12).

Figure 9b, presenting the carbon selectivities during these experiments, shows that again CO, CO₂, CH₄ and CH₃CHO were the main products, indicative of the activity of Ni in ethanol dehydrogenation and C-C bond rupture reactions. Selectivities of CO, CO₂ and CH₄ increased with contact time, while that of CH₃CHO decreased, consistent with the primary nature of CH₃CHO and the secondary nature of CO, CH₄ and CO₂. Given the lack of steam in these experiments, the presence of CO₂ bears discussion, and can potentially be attributed to the Boudouard reaction (11) or the oxidation of carbonaceous deposits by oxygen species originating from the adsorbed species, as also suggested by Fatsikostas and Verykios.³⁵

Finally, it is noteworthy that at a given ethanol conversion the CH₃CHO selectivity has approximately the same value for all W/F variation experiments in both reforming and decomposition modes, with the parameter showing a clear decreasing trend as conversion increases (Figure 10). This provides further evidence on the primary nature of CH₃CHO and proof that its formation pathway does not involve steam derived intermediates, as discussed previously. Even more striking and uncommon is the temperature independence observed in the selectivity trend, which suggests that the barrier of ethanol dehydrogenation is not particularly high, in line with limited relevant literature data available reporting a value as low as 32 kJ mol⁻¹, although on Ir versus Ni.¹⁵

3.4. *Time-on-stream performance*

Time-on-stream experiments were conducted to investigate the stability of the catalyst. Figure 11a presents the evolution with time-on-stream of ethanol conversion at 500°C and a S/C ratio of 3. The same experiment was carried out three times under these conditions, resulting in identical behaviour, proving the repeatability of the data. Ethanol conversion values towards either gaseous products only or towards all products are presented, as the times at which gas and liquid sampling took place were not the same. The catalytic reaction performance is stable over the whole duration tested. Looking at the gas-based data, there appears to be a reduction in activity or at least a drop in ethanol conversion to gaseous products in the first 30-40 minutes of reaction, followed by a long

term stability period. This drop could be linked to an initial coke formation period, when the free active site density is high, followed by a gradual drop as some of catalyst's active sites become blocked and coke removal reactions, e.g. gasification, become more competitive.⁵¹ It should be noted again that all kinetic data presented in previous sections were collected during this period of stable catalyst performance, while performance under the control conditions at the end of the sessions was always used to ascertain that the catalyst had not undergone deactivation (see Section 2.3).

The evolution with time-on-stream of gas-based and total product carbon selectivities is shown in Figure 11b. Performance was stable throughout the experimental run, while, as discussed previously, the high operating temperature of 500°C leads to high activity for the water-gas shift and methane steam reforming reactions as evident from the low CO and CH₄ and high CO₂ selectivities. The CH₃CHO selectivity was also stable and very low consistent with previous results, which explains the very similar gas-based and total ethanol conversion values presented in Figure 11c. A gradual and simultaneous increase in CO and decrease in CO₂ selectivities indicates a slight decrease in water-gas shift activity with time-on-stream, most probably due to slow catalyst deactivation by coking. Very similar observations were made during ESR time-on-stream experiments in a fluidised bed over Ni/SiO₂,¹⁹ suggesting, a particular effect of coking on the water-gas shift reaction. Nonetheless, H₂ yield presented in Figure 11a is overall stable and follows conversion trends, indicating the relatively small impact of the water-gas shift drop in activity to the overall H₂ production.

Following the above experiments, the catalyst was oxidised *in situ* under a flow of air at 700°C for 1.5 h to remove any coke deposits formed and was re-reduced at 500°C using a flow of 5 % H₂ on N₂ for 1 h. Catalytic activity was subsequently checked under the same conditions as above, with panel (a) of Figure 12 presenting the total and gas-based ethanol conversion evolution and panels (b) and (c) showing the gas-based and total carbon selectivities, respectively, versus time-on-stream. A

relatively stable performance is again observed, however when compared with that of the fresh catalyst sample, a lower activity is noted with total conversion stabilising at about 45 %, whereas previously it was maintained above 50 %. It is believed that the high temperature used during the *in situ* coke removal oxidation procedure resulted in a degree of sintering of the Ni particles, leading to a loss of effective catalytic surface area, affecting the activity of the catalyst.⁵² Moreover, a larger difference between total and gas-based ethanol conversion can be observed, also evident from the higher selectivity towards CH₃CHO, which with the fresh catalyst was less than 2 %, whereas in the regenerated case, it approached 10 %. Considering again Figure 10 and the related discussion in Section 3.2.2, the observed CH₃CHO selectivity value with the fresh catalyst is well in agreement with the overall trend of the parameter versus ethanol conversion. However, the value obtained with the regenerated catalyst deviates from this trend to a level that cannot be attributed to experimental error. These observations suggest that ethanol dehydrogenation is most probably a structure sensitive reaction, occurring preferentially at low coordination sites that reduced in number after sintering. Again though, due to the high temperature studied, the alternate ethanol decomposition pathway not involving acetaldehyde remains active, as the impact on overall conversion is not as high.

The effects of the regeneration treatment can also be observed from the trends of CO and CO₂ selectivities, which, as before, display a gradual respective increase and decrease, although this time at a faster rate. Particle aggregation via sintering influences the resistance of the catalyst towards coking, which could explain the more pronounced loss of water-gas shift reaction activity with time-on-stream.⁵³ Interestingly though, CH₄ selectivity appears not to be influenced by these effects and is equally low and stable at about 2 % in experiments using either fresh or regenerated catalyst. The latter in combination with the results obtained with the fresh catalyst suggest a comparatively stronger structure sensitivity or site specificity for the water-gas shift reaction. This could be linked, for example, with a requirement for (a specific type of) low-coordinated sites for the C-O bond formation,⁵⁴ which reduce in number both via sintering and are gradually blocked via coking, in

comparison to the C-C and C-H bonds cleavage involved in the conversion of oxygenates or hydrocarbons conversion reactions.

3.5. *Temperature programmed analyses of spent catalysts*

3.5.1. Temperature Programmed Oxidation (TPO)

TPO experiments were performed on Ni/SiO₂ spent catalyst samples collected after the time-on-stream experiments described above with both the originally fresh and the regenerated catalyst to identify the amount and type of coke deposited on each. The CO₂ evolution profiles obtained, normalised per unit mass of catalyst, are shown in Figure 13, while Table 2 presents the amount of carbon deposited on the catalyst bed. The latter was measured also via LECO elemental analysis on selected samples, with results being in very good agreement with the equivalent TPO ones (Table 2). No CO was detected in any TPO experiments, while a single CO₂ peak was observed, indicating the presence of one dominant coke type on the catalyst surface. The TPO profiles indicate certain differences though, with the fresh catalyst showing a peak in the CO₂ signal at 600°C, while for the regenerated catalyst the same peak appears at 540°C. In both cases, the high temperature indicates the presence of filamentous coke deposits that are potentially of a graphitic nature.⁵⁵ Elemental analysis showed a very high C/H ratio, exceeding 100 for both samples, suggesting highly dehydrogenated deposits, consistent with coke of a graphitic nature. Preliminary SEM analyses of these samples (not shown) further revealed the existence of a large amount of filaments in line with previously studies^{21,27,29,56,57} and in support of the TPO results. The amount of carbon deposited, either per unit ethanol fed during the 4 h experiments, or per catalyst mass, was also lower on the regenerated sample than the fresh, (Table 2), which can be related to the lower ethanol conversion obtained during the time-on-stream experiment with that sample. The latter implies an overall similar coking rate in comparison to the time-on-stream experiment with fresh catalyst. The lower temperature needed to remove coke on the regenerated sample could suggest a different reactivity or a lower degree of graphitisation, that could be linked with the sintering effects described in

Section 3.4 impacting also on the structure sensitive coke formation mechanism.^{58,59} Nonetheless, in these TPO tests, the mass of the regenerated catalyst sample used for analysis was half that of the fresh one, while O₂ concentration and flow were the same, so it is possible that the temperature peak difference is also affected by this. It has indeed been suggested that besides particle size and morphology, catalyst mass, O₂ concentration and heating rate can affect TPO profiles.⁶⁰ More evidence in support of the former explanation and suggesting indeed a difference in degree of graphitization between the two samples is provided in the following section.

3.5.2. Temperature Programmed Hydrogenation (TPH)

TPH experiments were performed on the same spent Ni/SiO₂ catalyst samples to further investigate the nature of carbonaceous deposits.⁶¹ Figure 14 presents the TPH profiles for the two catalyst samples, again normalised per unit mass of catalyst, while the amount of carbon removed as CH₄ from the catalyst bed is given in Table 3 and compared to that removed as CO₂ during TPO. The high temperature at which both TPH signals evolve their peaks again suggest that carbonaceous deposits are filamentous and have a certain degree of graphitization in agreement with the TPO results. It is also noteworthy that the amount of carbon that can be hydrogenated represents only a small fraction of what can be oxidized by TPO. About 8 % and 3 % of the total carbon deposits could be converted to CH₄ for the case of the fresh and regenerated samples, respectively. Additional TPO tests performed after each TPH experiment (Table 3) efficiently removed the remaining coke, with the carbon balance closing satisfactorily within experimental error at approximately 95 %, confirming that the major part of carbon deposits is non-reactive towards hydrogen. These TPO results after the TPH analyses agreed to those presented previously, in particular in relation to the regenerated sample evolving its peak at a lower temperature in comparison to the fresh sample, further evidencing that certain differences in the nature of coke deposited, or its reactivity, exist between these samples. Various studies⁶²⁻⁶⁴ have suggested that larger Ni particles favour the deposition of graphitic carbon and lead to filaments of greater size, which could be linked to the sintering caused by the *in situ* regeneration. Moreover, Figure 14 shows that a slightly different

temperature is required to hydrogenate the coke on the regenerated sample, in line with the above observations, although the small amount of carbon removed as CH_4 should be considered. TPH analysis further revealed in both samples that a very small amount of coke is more reactive to hydrogen, as suggested by the minor peaks visible at lower temperatures. These peaks correspond to the hydrogenation of deposits of amorphous nature that are capable of encapsulating active sites, limiting activity. The time-on-stream effects discussed in the previous section, in particular to the water-gas shift reaction, may be related to the formation of these deposits.

4. Conclusions

The kinetics of ethanol steam reforming were investigated on a Ni/SiO_2 catalyst in order to elucidate the reaction mechanism over a wide range of conditions. In agreement with literature on a variety of other metals, CH_3CHO was revealed to be a major intermediate in the reaction pathway of ESR through the dehydrogenation of ethanol. Below 450°C direct decomposition reactions of both ethanol and CH_3CHO are dominant, with limited participation of methanation, reforming or water-gas shift reactions, leading to the production of CH_4 and CO with high selectivities. In this temperature range, variation of space time allows CH_3CHO to be identified as the only primary product, with CO , CO_2 and CH_4 being secondary products. Ethanol conversion is found to be 0.5 order in ethanol and slightly negative in water partial pressure, evidencing that the dissociation/dehydrogenation of an ethanol derived intermediate is the rate determining step, with no participation of steam or its fragments. The competitive adsorption on the same active sites of water and ethanol even leads to saturation of the catalyst surface and decrease of the ethanol turnover frequency at high steam partial pressures. At higher temperatures, methane steam reforming and the water-gas shift become promoted, enhancing the production of H_2 and CO_2 . The acceleration of all decomposition and dehydrogenation reactions in this regime even leads to CO and CH_4 appearing as primary products, along with CH_3CHO , with results suggesting the possibility of an alternate pathway not involving CH_3CHO becoming dominant. CO_2 , although predominantly a

secondary product of CO, is possibly also formed by the dissociation of acetate species, with traces of acetic acid in the products consistent with such a proposal, or even via the Boudouard reaction in the absence of steam. TPO and TPH analyses of spent catalyst samples suggest that the carbon deposits are graphitic in nature and filamentous type of coke is formed, which explains the stable catalytic performance during time-on-stream experiments.

Conflicts of interest

There are no conflicts to declare.

Bibliography

- 1 P. N. Kechagiopoulos, S. S. Voutetakis, A. A. Lemonidou and I. A. Vasalos, Sustainable hydrogen production via reforming of ethylene glycol using a novel spouted bed reactor, *Catal. Today*, 2007, **127**, 246–255.
- 2 O. A. Olafadehan, A. A. Ayoola, O. O. Akintunde and V. O. Adeniyi, Mechanistic Kinetic Models for Steam Reforming of concentrated crude ethanol on Ni/Al₂O₃ catalyst, *J. Eng. Sci. Technol.*, 2015, **10**, 633–653.
- 3 V. I. Popa, in *Biomass as Renewable Raw Material to Obtain Bioproducts of High-Tech Value*, eds. V. Popa and I. Volf, Elsevier, 1st edn., 2018, pp. 1–37.
- 4 J. Chen, J. Sun and Y. Wang, Catalysts for Steam Reforming of Bio-oil: A Review, *Ind. Eng. Chem. Res.*, 2017, **56**, 4627–4637.
- 5 P. N. Kechagiopoulos, S. S. Voutetakis, A. A. Lemonidou and I. A. Vasalos, Hydrogen production via steam reforming of the aqueous phase of bio-oil in a fixed bed reactor, *Energy and Fuels*, 2006, **20**, 2155–2163.
- 6 S. Czernik, R. French, C. Feik and E. Chornet, Hydrogen by catalytic steam reforming of liquid byproducts from biomass thermoconversion processes, *Ind. Eng. Chem. Res.*, 2002, **41**, 4209–4215.
- 7 L. Barattini, G. Ramis, C. Resini, G. Busca, M. Sisani and U. Costantino, Reaction path of ethanol and acetic acid steam reforming over Ni-Zn-Al catalysts. Flow reactor studies, *Chem. Eng. J.*, 2009, **153**, 43–49.
- 8 Y. J. Wu, J. C. Santos, P. Li, J. G. Yu, A. F. Cunha and A. E. Rodrigues, Simplified kinetic model for steam reforming of ethanol on a Ni/Al₂O₃ catalyst, *Can. J. Chem. Eng.*, 2014, **92**, 116–130.
- 9 J. Sun, X. P. Qiu, F. Wu and W. T. Zhu, H₂ from steam reforming of ethanol at low temperature over Ni/Y₂O₃ and Ni/La₂O₃ catalysts for fuel-cell application, *Int. J. Hydrogen Energy*, 2005, **30**, 437–445.
- 10 M. Levent, M. Ağbaba and Y. Şahin, Production of Synthesis Gases from Ethanol Steam Reforming Process, *Int. J. Clean Coal Energy*, 2016, **5**, 45–63.
- 11 D. A. Morgenstern and J. P. Fornango, Low-temperature reforming of ethanol over copper-plated raney nickel: A new route to sustainable hydrogen for transportation, *Energy and Fuels*, 2005, **19**, 1708–1716.
- 12 E. Örucü, F. Gökalliler, A. E. Aksoylu and Z. I. Önsan, Ethanol steam reforming for hydrogen production over bimetallic Pt-Ni/Al₂O₃, *Catal. Letters*, 2008, **120**, 198–203.
- 13 G. Zeng, Y. Li and U. Olsbye, Kinetic and process study of ethanol steam reforming over Ni/Mg(Al)O catalysts: The initial steps, *Catal. Today*, 2015, **259**, 312–322.
- 14 B. Roy, U. Martinez, K. Loganathan, A. K. Datye and C. A. Leclerc, Effect of preparation methods on the performance of Ni/Al₂O₃ catalysts for aqueous-phase reforming of ethanol: Part I-catalytic activity, *Int. J. Hydrogen Energy*, 2012, **37**, 8143–8153.
- 15 F. Wang, W. Cai, C. Descorme, H. Provendier, W. Shen, C. Mirodatos and Y. Schuurman, From mechanistic to kinetic analyses of ethanol steam reforming over Ir/CeO₂ catalyst, *Int. J. Hydrogen Energy*, 2014, **39**, 18005–18015.

- 16 I. Llera, V. Mas, M. L. Bergamini, M. Laborde and N. Amadeo, Bio-ethanol steam reforming on Ni based catalyst. Kinetic study, *Chem. Eng. Sci.*, 2012, **71**, 356–366.
- 17 C. M. A. Parlett, A. Aydin, L. J. Durdell, L. Frattini, M. A. Isaacs, A. F. Lee, X. Liu, L. Olivi, R. Trofimovaite, K. Wilson and C. Wu, Tailored mesoporous silica supports for Ni catalysed hydrogen production from ethanol steam reforming, *Catal. Commun.*, 2017, **91**, 76–79.
- 18 A. Akande, A. Aboudheir, R. Idem and A. Dalai, Kinetic modeling of hydrogen production by the catalytic reforming of crude ethanol over a co-precipitated Ni - Al₂O₃ catalyst in a packed bed tubular reactor, *Int. J. Hydrogen Energy*, 2006, **31**, 1707–1715.
- 19 M. C. Sanchez-Sanchez, R. M. Navarro Yerga, D. I. Kondarides, X. E. Verykios and J. L. G. Fierro, Mechanistic Aspects of the Ethanol Steam Reforming Reaction for Hydrogen Production on Pt, Ni, and PtNi Catalysts Supported on γ -Al₂O₃, *J. Phys. Chem. A*, 2010, **114**, 3873–3882.
- 20 J. E. Sutton, P. Panagiotopoulou, X. E. Verykios and D. G. Vlachos, Combined DFT, microkinetic, and experimental study of ethanol steam reforming on Pt, *J. Phys. Chem. C*, 2013, **117**, 4691–4706.
- 21 J. Vicente, J. Ereña, C. Montero, M. J. Azkoiti, J. Bilbao and A. G. Gayubo, Reaction pathway for ethanol steam reforming on a Ni/SiO₂ catalyst including coke formation, *Int. J. Hydrogen Energy*, 2014, **39**, 18820–18834.
- 22 L. C. Chen and S. D. Lin, The ethanol steam reforming over Cu-Ni/SiO₂ catalysts: Effect of Cu/Ni ratio, *Appl. Catal. B Environ.*, 2011, **106**, 639–649.
- 23 V. Nichele, M. Signoretto, F. Pinna, F. Menegazzo, I. Rossetti, G. Cruciani, G. Cerrato and A. Di Michele, Ni/ZrO₂ catalysts in ethanol steam reforming: Inhibition of coke formation by CaO-doping, *Appl. Catal. B Environ.*, 2014, **150–151**, 12–20.
- 24 V. Palma, F. Castaldo, P. Ciambelli and G. Iaquaniello, CeO₂-supported Pt/Ni catalyst for the renewable and clean H₂ production via ethanol steam reforming, *Appl. Catal. B Environ.*, 2014, **145**, 73–84.
- 25 T. Hou, B. Yu, S. Zhang, T. Xu, D. Wang and W. Cai, Hydrogen production from ethanol steam reforming over Rh/CeO₂ catalyst, *Catal. Commun.*, 2015, **58**, 137–140.
- 26 I. Rossetti, J. Lasso, V. Nichele, M. Signoretto, E. Finocchio, G. Ramis and A. Di Michele, Silica and zirconia supported catalysts for the low-temperature ethanol steam reforming, *Appl. Catal. B Environ.*, 2014, **150–151**, 257–267.
- 27 C. Wu and P. T. Williams, A Novel Nano-Ni/SiO₂ Catalyst for Hydrogen Production from Steam Reforming of Ethanol, *Environ. Sci. Technol.*, 2010, **44**, 5993–5998.
- 28 L. Liu, X. Ma and J. Li, Hydrogen production from ethanol steam reforming over Ni/SiO₂ catalysts: A comparative study of traditional preparation and microwave modification methods, *Int. J. Energy Res.*, 2014, **38**, 860–874.
- 29 C. Wu, V. Dupont, M. A. Nahil, B. Dou, H. Chen and P. T. Williams, Investigation of Ni/SiO₂ catalysts prepared at different conditions for hydrogen production from ethanol steam reforming, *J. Energy Inst.*, 2017, **90**, 276–284.
- 30 M. A. Vannice, *Kinetics of Catalytic Reactions*, Springer, 2005.
- 31 P. B. Weisz and C. D. Prater, Interpretation of Measurements in Experimental Catalysis, *Adv.*

- Catal.*, 1954, **6**, 143–196.
- 32 S. D. Angeli, F. G. Pilitsis and A. A. Lemonidou, Methane steam reforming at low temperature: Effect of light alkanes' presence on coke formation, *Catal. Today*, 2015, **242**, 119–128.
- 33 S. D. Angeli, L. Turchetti, G. Monteleone and A. A. Lemonidou, Catalyst development for steam reforming of methane and model biogas at low temperature, *Appl. Catal. B Environ.*, 2016, **181**, 34–46.
- 34 M. Benito, J. L. Sanz, R. Isabel, R. Padilla, R. Arjona and L. Daza, Bio-ethanol steam reforming: Insights on the mechanism for hydrogen production, *J. Power Sources*, 2005, **151**, 11–17.
- 35 A. N. Fatsikostas and X. E. Verykios, Reaction network of steam reforming of ethanol over Ni-based catalysts, *J. Catal.*, 2004, **225**, 439–452.
- 36 M. Dömök, M. Tóth, J. Raskó and A. Erdohelyi, Adsorption and reactions of ethanol and ethanol-water mixture on alumina-supported Pt catalysts, *Appl. Catal. B Environ.*, 2007, **69**, 262–272.
- 37 S. Martí, N. Homs, E. B. Pereira and P. Ramírez de la Piscina, Catalytic behavior of unsupported Co materials in the reformation of ethanol to hydrogen: An in situ diffuse reflectance infrared Fourier transform (DRIFT)-mass spectrometry study, *Pure Appl. Chem.*, 2008, **80**, 2397–2403.
- 38 J. A. Anderson and C. H. Rochester, Infrared study of the adsorption of acetone, acrolein, ethanoic acid and propene-NO mixtures on Rh/Al₂O₃ catalysts, *J. Chem. Soc. Faraday Trans. 1 Phys. Chem. Condens. Phases*, 1989, **85**, 1117–1128.
- 39 A. F. Cunha, Y. J. Wu, J. C. Santos and A. E. Rodrigues, Steam reforming of ethanol on copper catalysts derived from hydrotalcite-like materials, *Ind. Eng. Chem. Res.*, 2012, **51**, 13132–13143.
- 40 A. K. Yadav and P. D. Vaidya, Kinetic investigation on butanol steam reforming over Ru/Al₂O₃ catalyst, *Int. J. Hydrogen Energy*, 2017, **42**, 25203–25212.
- 41 P. Ciambelli, V. Palma and A. Ruggiero, Low temperature catalytic steam reforming of ethanol. 2. Preliminary kinetic investigation of Pt/CeO₂ catalysts, *Appl. Catal. B Environ.*, 2010, **96**, 190–197.
- 42 I. J. Oluku, H. Ibrahim and R. Idem, Kinetic Study of Hydrogen Production by the High Temperature Water Gas Shift Reaction of Reformate Gas in Conventional and Membrane Packed Bed Reactors over Ca-Promoted CeO₂-ZrO₂ Supported Ni-Cu Catalyst, *Ind. Eng. Chem. Res.*, 2015, **54**, 612–622.
- 43 L. Bobrova, D. Andreev, E. Ivanov, N. Mezentseva, M. Simonov, L. Makarshin, A. Gribovskii and V. Sadykov, Water-Gas shift reaction over Ni/CeO₂ catalysts, *Catalysts*, 2017, **7**, 310.
- 44 J. Y. Lim, J. McGregor, A. J. Sederman and J. S. Dennis, The role of the Boudouard and water-gas shift reactions in the methanation of CO or CO₂ over Ni/γ-Al₂O₃ catalyst, *Chem. Eng. Sci.*, 2016, **152**, 754–766.
- 45 P. N. Kechagiopoulos, S. D. Angeli and A. A. Lemonidou, Low temperature steam reforming of methane: A combined isotopic and microkinetic study, *Appl. Catal. B Environ.*, 2017, **205**, 238–253.

- 46 J. Wei and E. Iglesia, Isotopic and kinetic assessment of the mechanism of reactions of CH₄ with CO₂ or H₂O to form synthesis gas and carbon on nickel catalysts, *J. Catal.*, 2004, **224**, 370–383.
- 47 A. Simson, E. Waterman, R. Farrauto and M. Castaldi, Kinetic and process study for ethanol reforming using a Rh/Pt washcoated monolith catalyst, *Appl. Catal. B Environ.*, 2009, **89**, 58–64.
- 48 C. Sprung, P. N. Kechagiopoulos, J. W. Thybaut, B. Arstad, U. Olsbye and G. B. Marin, Microkinetic evaluation of normal and inverse kinetic isotope effects during methane steam reforming to synthesis gas over a Ni/NiAl₂O₄ model catalyst, *Appl. Catal. A Gen.*, 2015, **492**, 231–242.
- 49 P. D. Vaidya and A. E. Rodrigues, Insight into steam reforming of ethanol to produce hydrogen for fuel cells, *Chem. Eng. J.*, 2006, **117**, 39–49.
- 50 S. J. Han, J. H. Song, Y. Bang, J. Yoo, S. Park, K. H. Kang and I. K. Song, Hydrogen production by steam reforming of ethanol over mesoporous Cu-Ni-Al₂O₃-ZrO₂ xerogel catalysts, *Int. J. Hydrogen Energy*, 2016, **41**, 2554–2563.
- 51 Z. Chen, Y. Yan and S. S. E. H. Elnashaie, Catalyst deactivation and engineering control for steam reforming of higher hydrocarbons in a novel membrane reformer, *Chem. Eng. Sci.*, 2004, **59**, 1965–1978.
- 52 S. M. Hashemnejad and M. Parvari, Deactivation and Regeneration of Nickel-Based Catalysts for Steam-Methane Reforming, *Chinese J. Catal.*, 2011, **32**, 273–279.
- 53 J. Sehested, J. A. P. Gelten, I. N. Remediakis, H. Bengaard and J. K. Nørskov, Sintering of nickel steam-reforming catalysts: effects of temperature and steam and hydrogen pressures, *J. Catal.*, 2004, **223**, 432–443.
- 54 R. A. Van Santen, Complementary Structure Sensitive and Insensitive Catalytic Relationships, *Acc. Chem. Res.*, 2009, **42**, 57–66.
- 55 R. Padilla, M. Benito, L. Rodríguez, A. Serrano, G. Muñoz and L. Daza, Nickel and cobalt as active phase on supported zirconia catalysts for bio-ethanol reforming: Influence of the reaction mechanism on catalysts performance, *Int. J. Hydrogen Energy*, 2010, **35**, 8921–8928.
- 56 P. H. Blanco, C. Wu, J. A. Onwudili, V. Dupont and P. T. Williams, Catalytic Pyrolysis/Gasification of Refuse Derived Fuel for Hydrogen Production and Tar Reduction: Influence of Nickel to Citric Acid Ratio Using Ni/SiO₂ Catalysts, *Waste and Biomass Valorization*, 2014, **5**, 625–636.
- 57 S. Y. Chin, Y. H. Chin and M. D. Amiridis, Hydrogen production via the catalytic cracking of ethane over Ni/SiO₂ catalysts, *Appl. Catal. A Gen.*, 2006, **300**, 8–13.
- 58 K. O. Christensen, D. Chen, R. Løvdeng and A. Holmen, Effect of supports and Ni crystal size on carbon formation and sintering during steam methane reforming, *Appl. Catal. A Gen.*, 2006, **314**, 9–22.
- 59 M. A. Goula, A. A. Lemonidou and A. M. Efstathiou, Characterization of Carbonaceous Species Formed during Reforming of CH₄ with CO₂ over Ni/CaO–Al₂O₃ Catalysts Studied by Various Transient Techniques, *J. Catal.*, 1996, **640**, 626–640.
- 60 C. Querini and S. C. Fung, Temperature-programmed oxidation technique: kinetics of coke-O₂

- reaction on supported metal catalysts, *Appl. Catal. A Gen.*, 1994, **117**, 53–74.
- 61 Q. Yan, H. Toghiani and M. G. White, Combined temperature-programmed processes, pulse reactions, and on-line mass spectroscopy study of CH₄, CO, and H₂ interaction with Ni/Al₂O₃ catalysts, *J. Phys. Chem. C*, 2007, **111**, 18646–18662.
- 62 J.-H. Kim, D. J. Suh, T. Park and K. Kim, Effect of metal particle size on coking during CO₂ reforming of CH₄ over Ni–alumina aerogel catalysts, *Appl. Catal. A Gen.*, 2000, **197**, 191–200.
- 63 H. S. Bengaard, J. K. Nørskov, J. Sehested, B. S. Clausen, L. P. Nielsen, A. M. Molenbroek and J. R. Rostrup-Nielsen, Steam Reforming and Graphite Formation on Ni Catalysts, *J. Catal.*, 2002, **209**, 365–384.
- 64 F. Frusteri, S. Freni, V. Chiodo, L. Spadaro, O. Di Blasi, G. Bonura and S. Cavallaro, Steam reforming of bio-ethanol on alkali-doped Ni/MgO catalysts: Hydrogen production for MC fuel cell, *Appl. Catal. A Gen.*, 2004, **270**, 1–7.

Table 1. Main reactions reported to occur during ESR.

$\text{CH}_3\text{CH}_2\text{OH} + 3\text{H}_2\text{O} \rightleftharpoons 6\text{H}_2 + 2\text{CO}_2$ (1)	$\text{CO} + \text{H}_2\text{O} \rightleftharpoons \text{CO}_2 + \text{H}_2$ (2)
$\text{CH}_3\text{CH}_2\text{OH} \rightleftharpoons \text{CH}_3\text{CHO} + \text{H}_2$ (3)	$\text{CH}_3\text{CH}_2\text{OH} \rightleftharpoons \text{CH}_4 + \text{CO} + \text{H}_2$ (4)
$\text{CH}_3\text{CHO} \rightleftharpoons \text{CH}_4 + \text{CO}$ (5)	$\text{CH}_4 + \text{H}_2\text{O} \rightleftharpoons \text{CO} + 3\text{H}_2$ (6)
$\text{CH}_4 + 2\text{H}_2\text{O} \rightleftharpoons \text{CO}_2 + 4\text{H}_2$ (7)	$\text{CH}_3\text{CH}_2\text{OH} \rightleftharpoons \text{C}_2\text{H}_4 + \text{H}_2\text{O}$ (8)
$\text{CH}_3\text{CHO} + \text{H}_2\text{O} \rightleftharpoons \text{CH}_3\text{COOH} + \text{H}_2$ (9)	$\text{CH}_3\text{COOH} \rightleftharpoons \text{CH}_4 + \text{CO}_2$ (10)
$2\text{CO} \rightleftharpoons \text{CO}_2 + \text{C}$ (11)	$\text{CH}_4 \rightarrow \text{C} + 2\text{H}_2$ (12)
$\text{C}_2\text{H}_4 \xrightarrow{\text{polymerisation}} \text{Coke}$ (13)	

Table 2. Mass based percentages of carbon deposited as coke on catalyst samples in terms of carbon fed and of catalyst mass after time-on-stream experiments using fresh and regenerated catalysts as determined via TPO and elemental analyses.

Catalyst sample	Coke/Carbon fed (TPO)	Coke/Catalyst mass (TPO)	Coke/Carbon fed (LECO)	Coke/Catalyst mass (LECO)
Fresh	3.22 %	67.59 %	3.16 %	66.33 %
Regenerated	3.06 %	64.29 %	-	-

Table 3. Mass of carbon removed from catalyst samples after time-on-stream experiments using fresh and regenerated catalysts as determined via TPO, TPH and TPO carried out after TPH analyses.

Catalyst sample	C (TPO)	C (TPH)	C (TPH)/C (TPO)	C (TPO after TPH)
Fresh	27.04 mg	2.21 mg	8.17 %	23.03 mg
Regenerated	25.71 mg	0.87 mg	3.38 %	23.72 mg

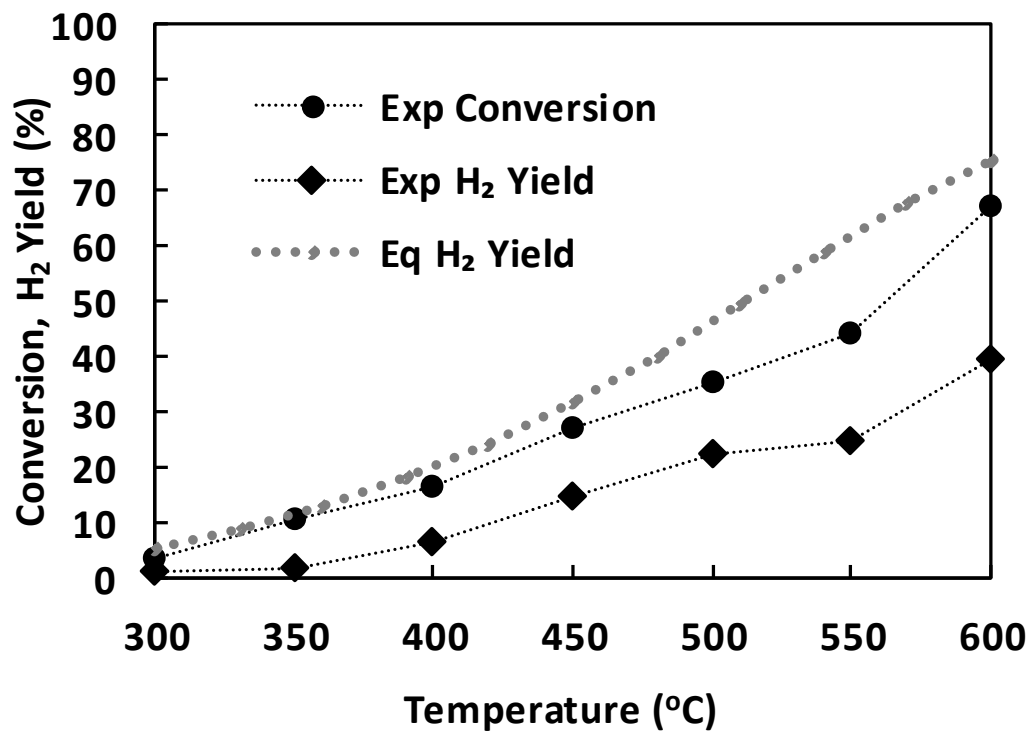


Figure 1. Temperature effect on ethanol conversion and hydrogen yield compared with equilibrium ($W/F_{\text{Eth},t0} = 91.88 \text{ g}_{\text{cat}} \text{ s g}_{\text{Eth}}^{-1}$, $P = 0.7 \text{ bar}$, $S/C = 3$).

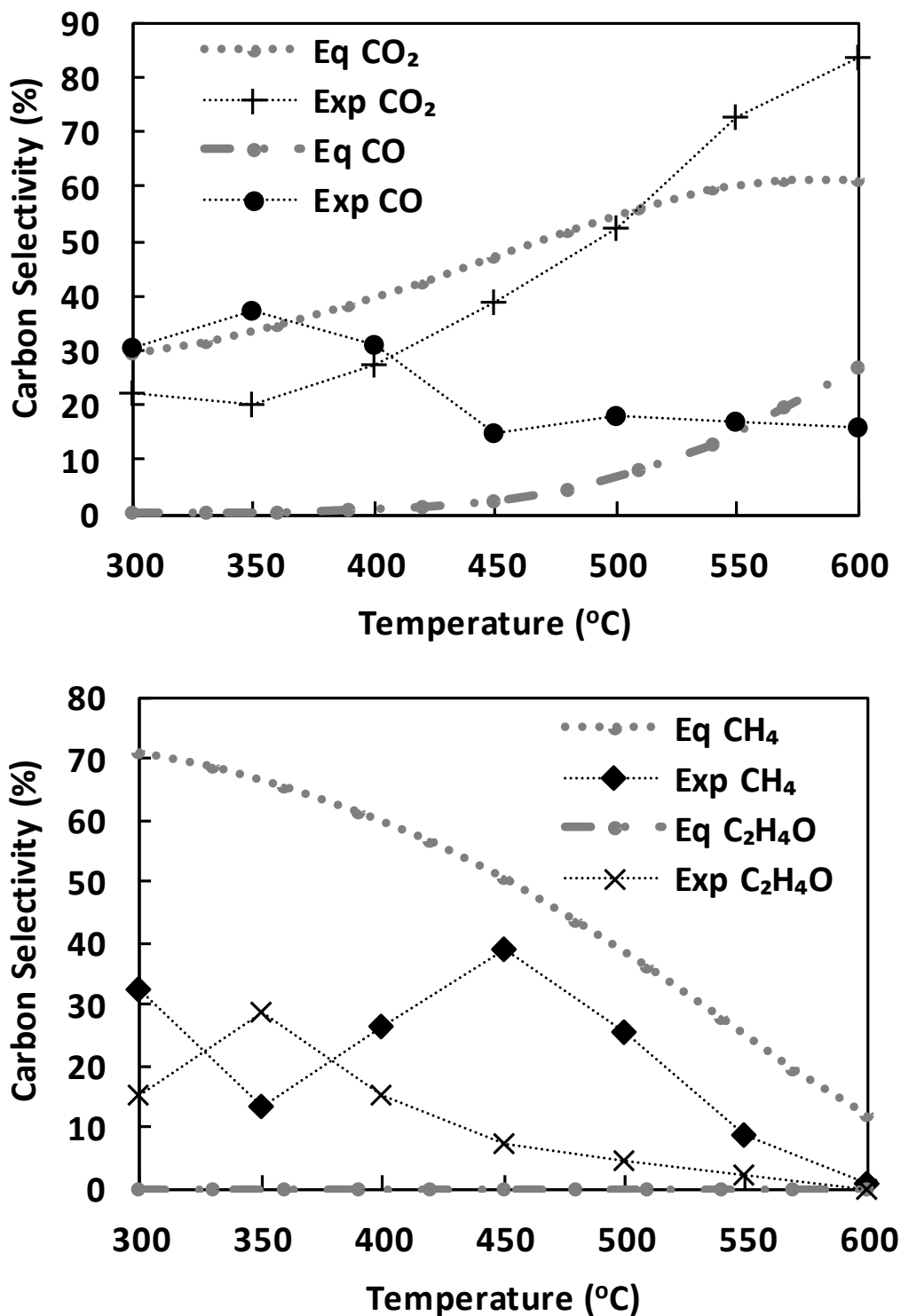


Figure 2. Temperature effect on carbon selectivities of CO, CO₂, CH₄ and C₂H₄O compared with equilibrium ($W/F_{\text{Eth},t0} = 91.88 \text{ g}_{\text{cat}} \text{ s g}_{\text{Eth}}^{-1}$, $P = 0.7 \text{ bar}$, $S/C = 3$).

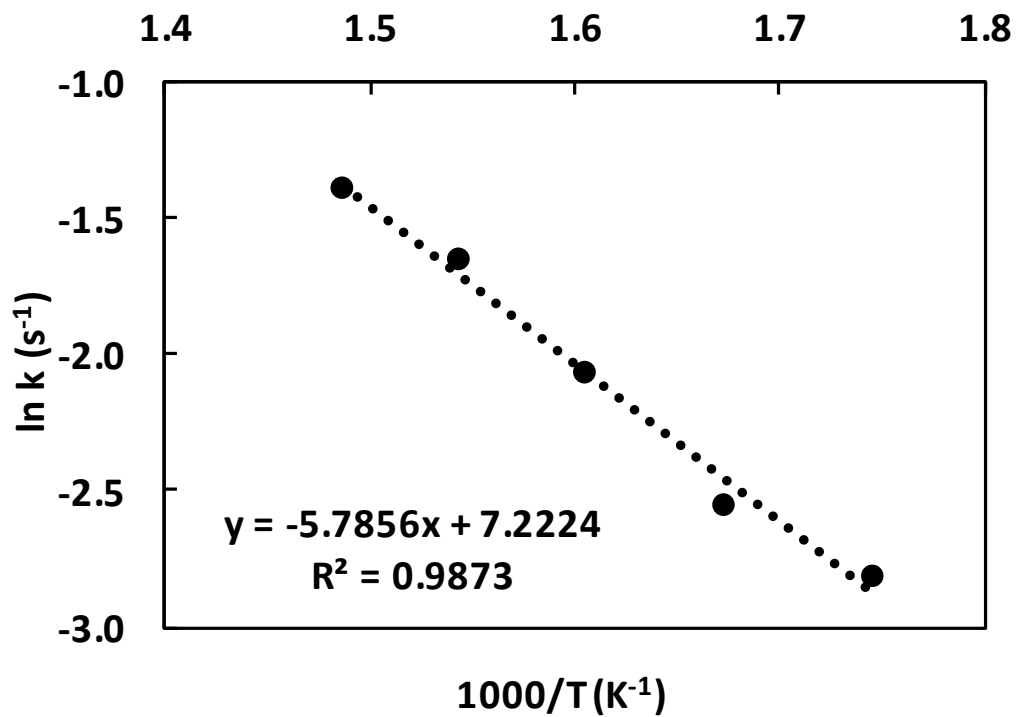


Figure 3. Arrhenius plot of ESR ($W/F_{\text{Eth},\text{to}} = 91.88 \text{ g}_{\text{cat}} \text{ s g}_{\text{Eth}}^{-1}$, $P = 0.7 \text{ bar}$, $S/C = 3$).

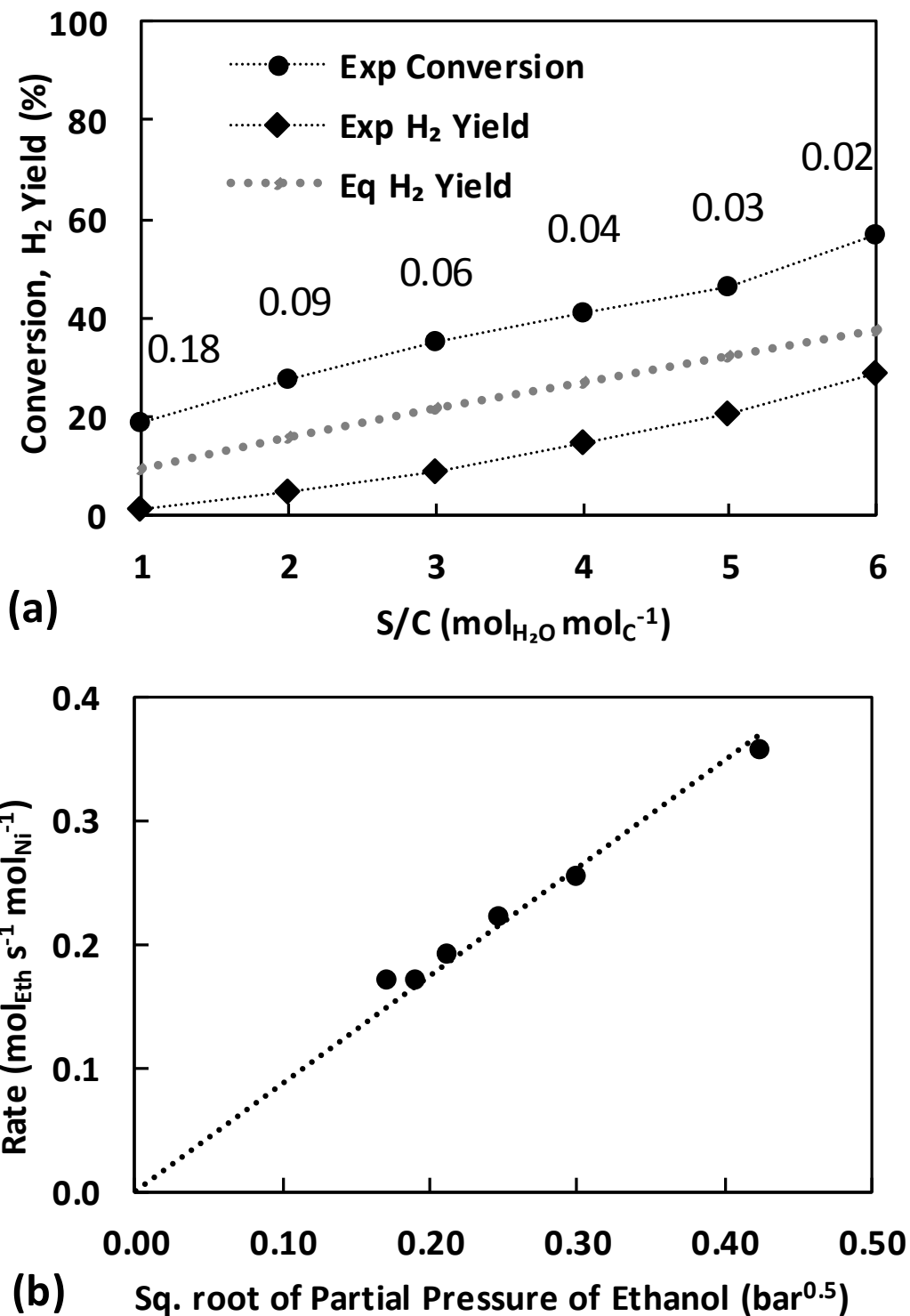


Figure 4. Partial pressure of ethanol effect on ethanol conversion and H₂ yield at 400°C presented as a S/C variation with numbers on plot annotating the equivalent partial pressures of ethanol in bar (a) and ESR reaction rate with respect to the square root of the ethanol partial pressure at 400°C (b) (P = 0.9 bar, V_{tot} = 160 cm³ min⁻¹).

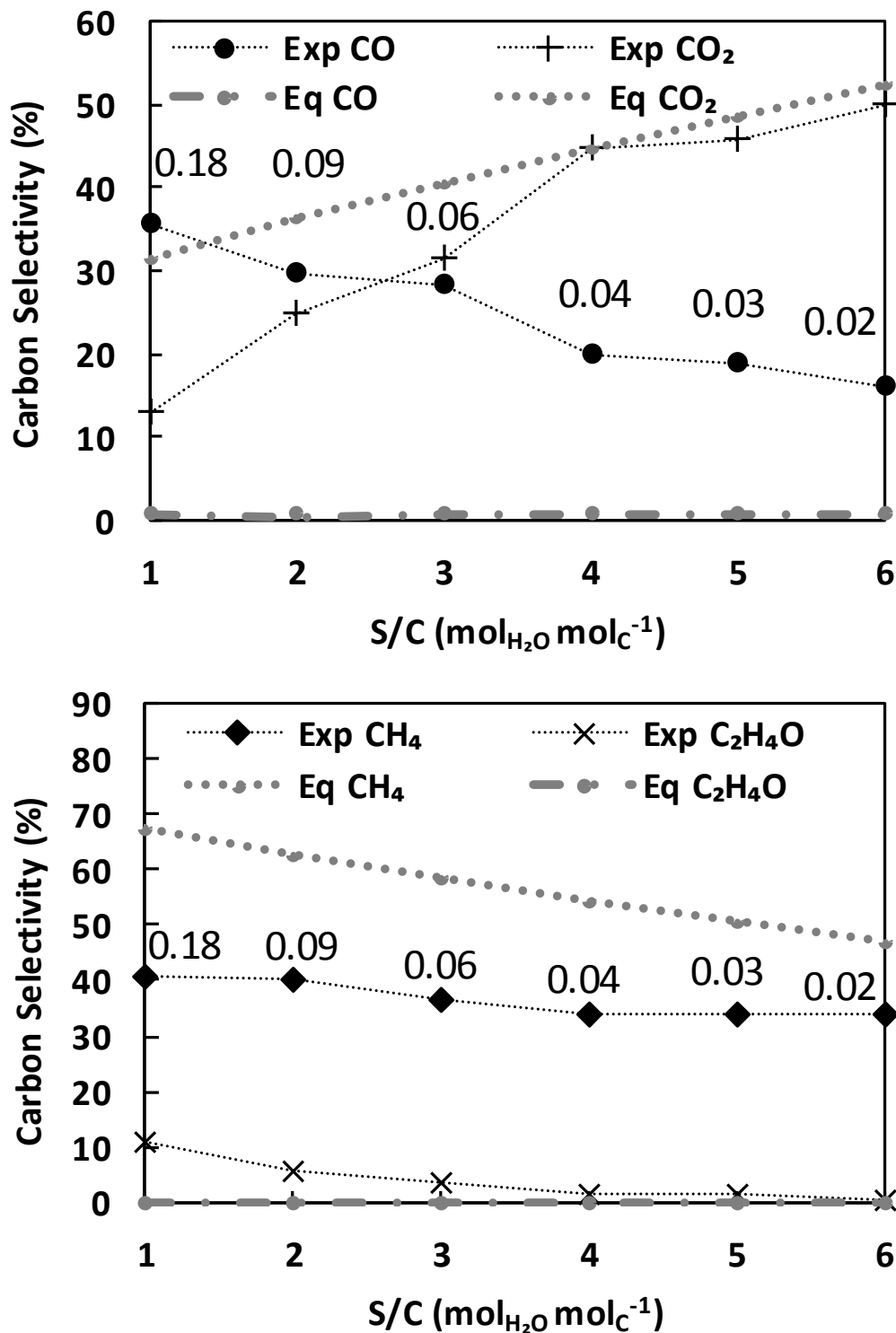


Figure 5. Partial pressure of ethanol effect on carbon selectivities of CO, CO₂, CH₄ and C₂H₄O at 400°C presented as a S/C variation with numbers on plot annotating the equivalent partial pressures of ethanol in bar ($P = 0.9$ bar, $V_{\text{tot}} = 160$ cm³ min⁻¹).

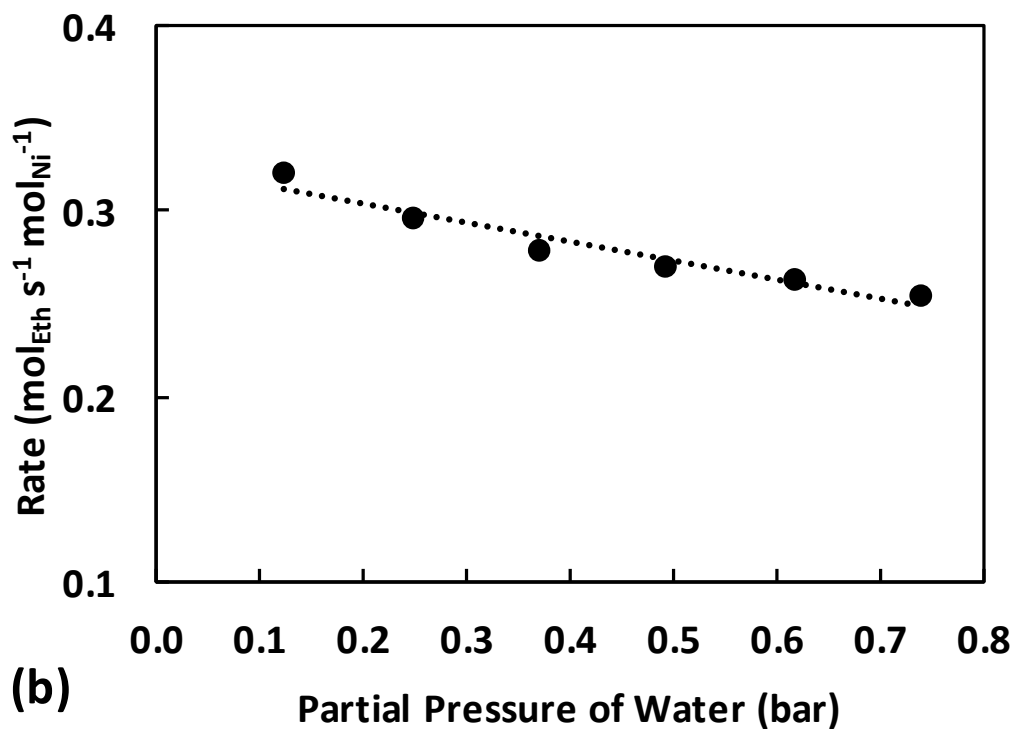
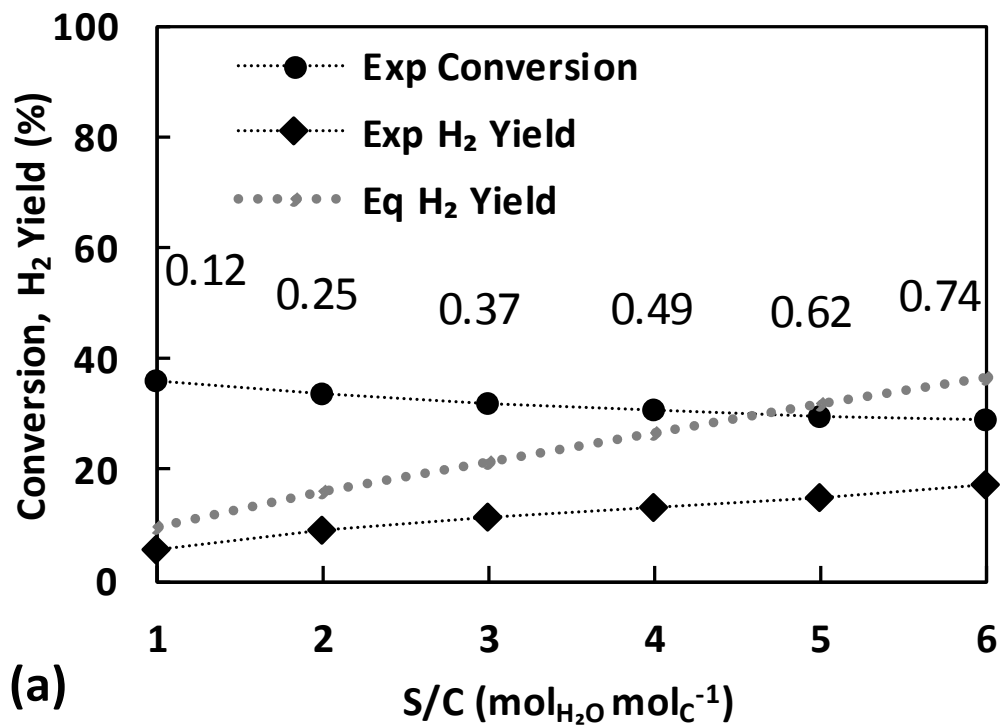


Figure 6. Partial pressure of water effect on ethanol conversion and H₂ yield at 400°C presented as a S/C variation with numbers on plot annotating the equivalent partial pressures of water in bar (a) and ESR reaction rate with respect to water partial pressure at 400°C (b) ($P = 0.9$ bar, $V_{\text{tot}} = 213$ cm³ min⁻¹).

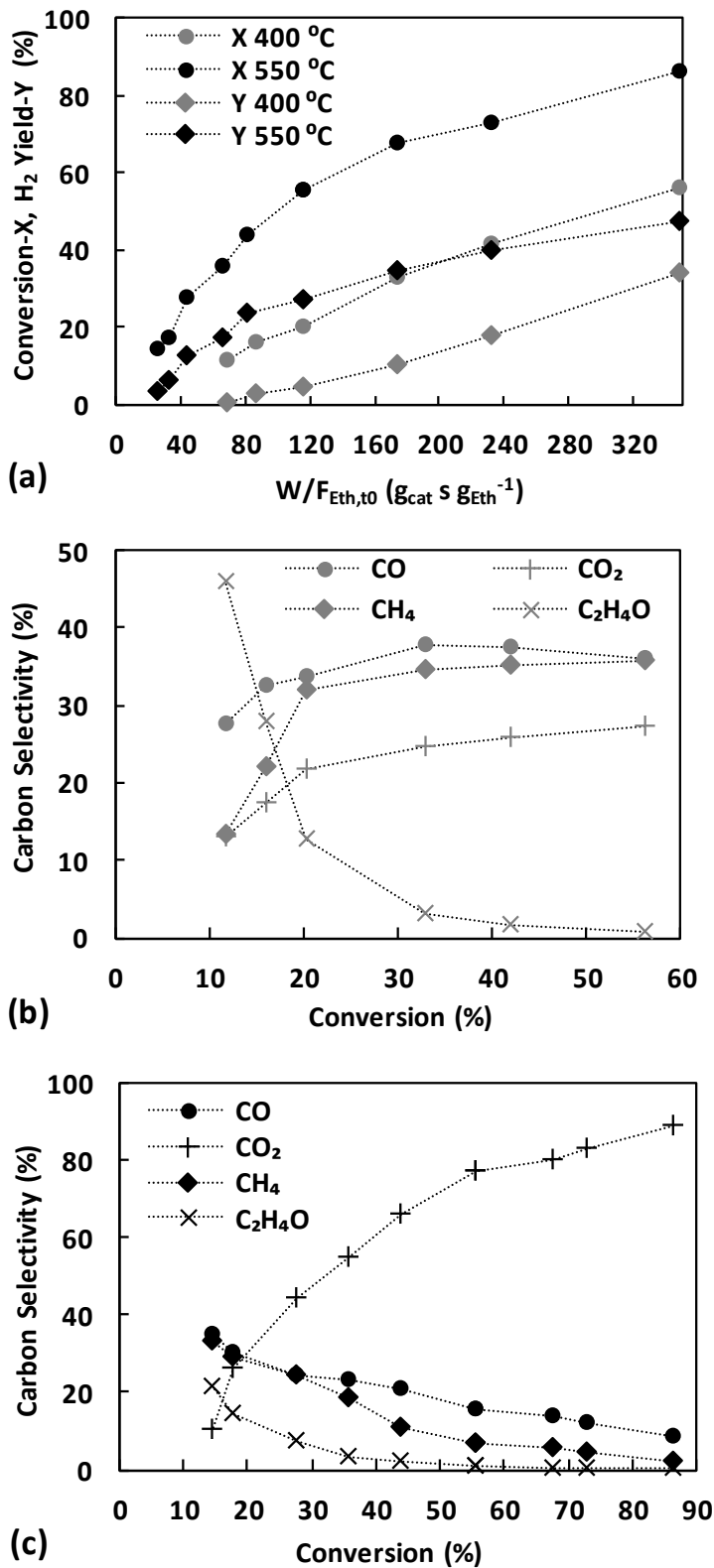


Figure 8. $W/F_{Eth,t0}$ effect on ethanol conversion and H_2 yield at 400 °C and 550 °C (a) and carbon selectivities of CO , CO_2 , CH_4 and C_2H_4O versus conversion observed during $W/F_{Eth,t0}$ variation at 400 °C (b) and 550 °C (c) ($P = 0.8$ bar, $S/C = 3$).

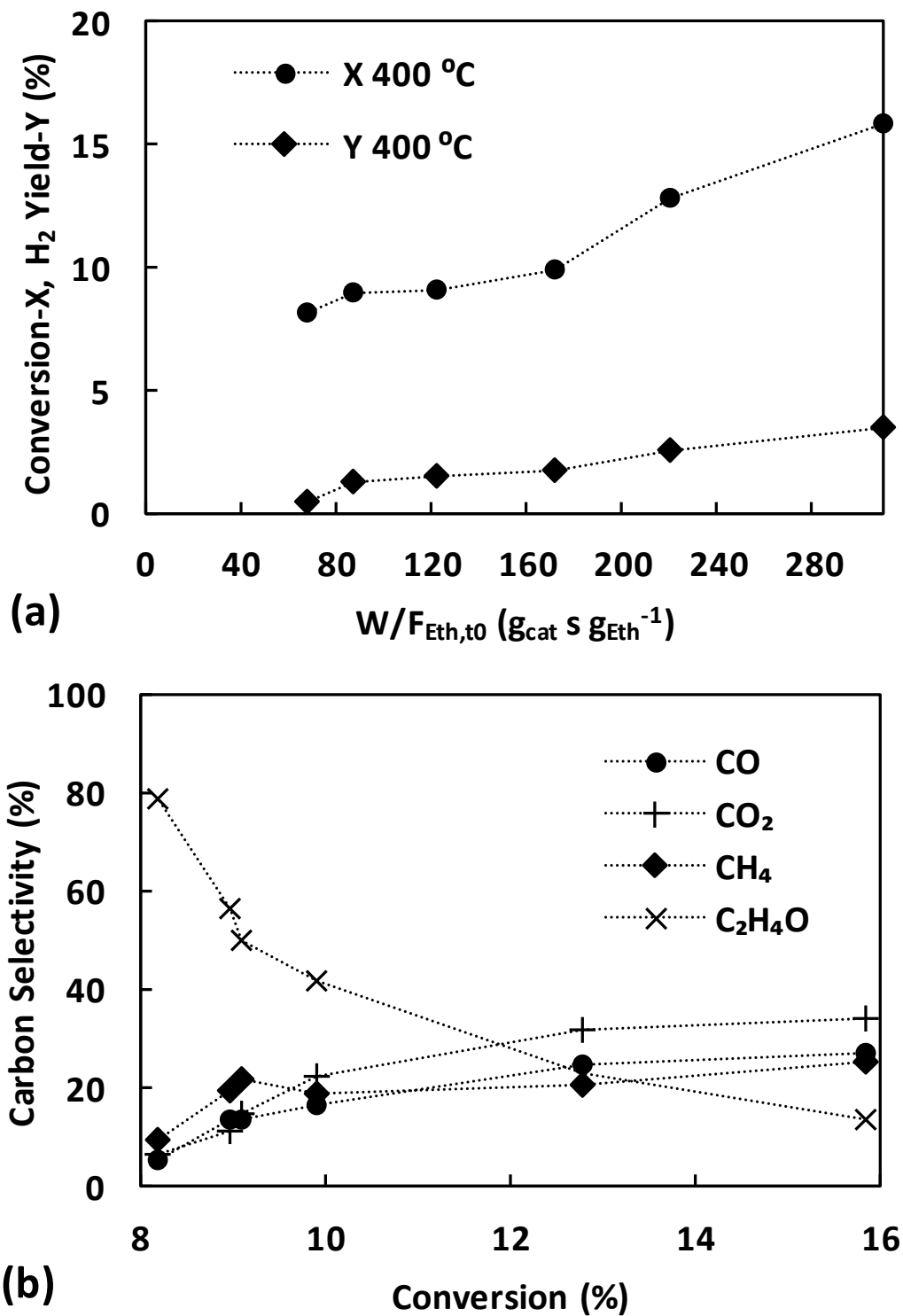


Figure 9. $W/F_{\text{Eth},t0}$ effect on the ethanol decomposition and H_2 yield (a) and carbon selectivities of CO , CO_2 , CH_4 and $\text{C}_2\text{H}_4\text{O}$ (b) at 400°C ($P = 0.8$ bar, $S/C = 3$).

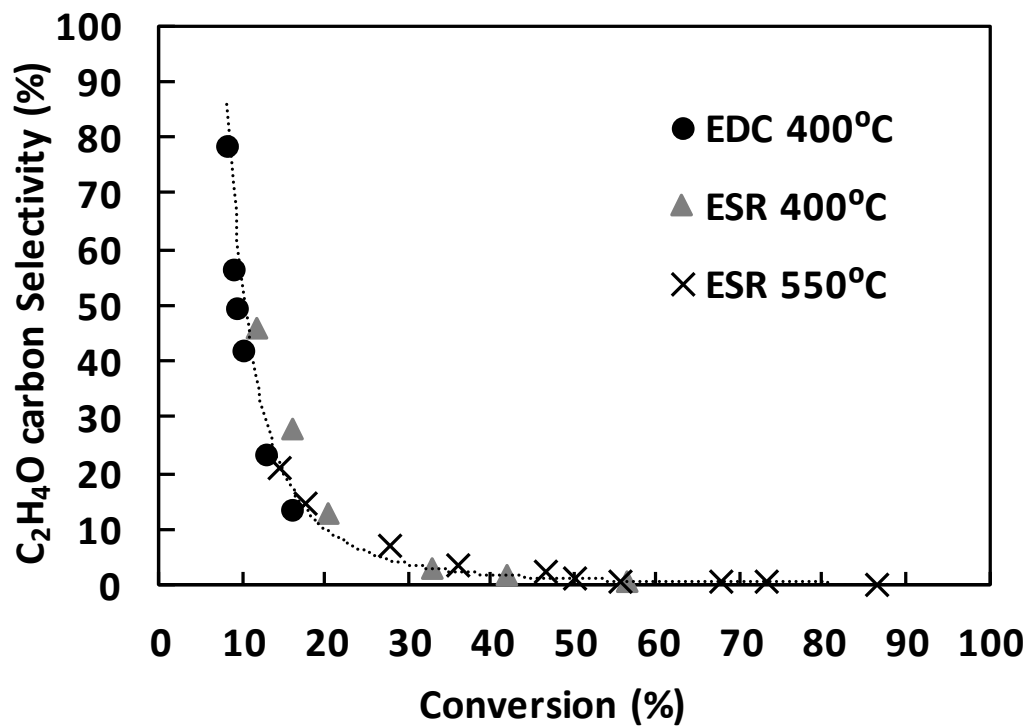


Figure 10. Acetaldehyde selectivity versus ethanol conversion during different $W/F_{Eth,t0}$ variation experiments at steam reforming and decomposition mode as described in Sections 3.2.1 and 3.2.2.

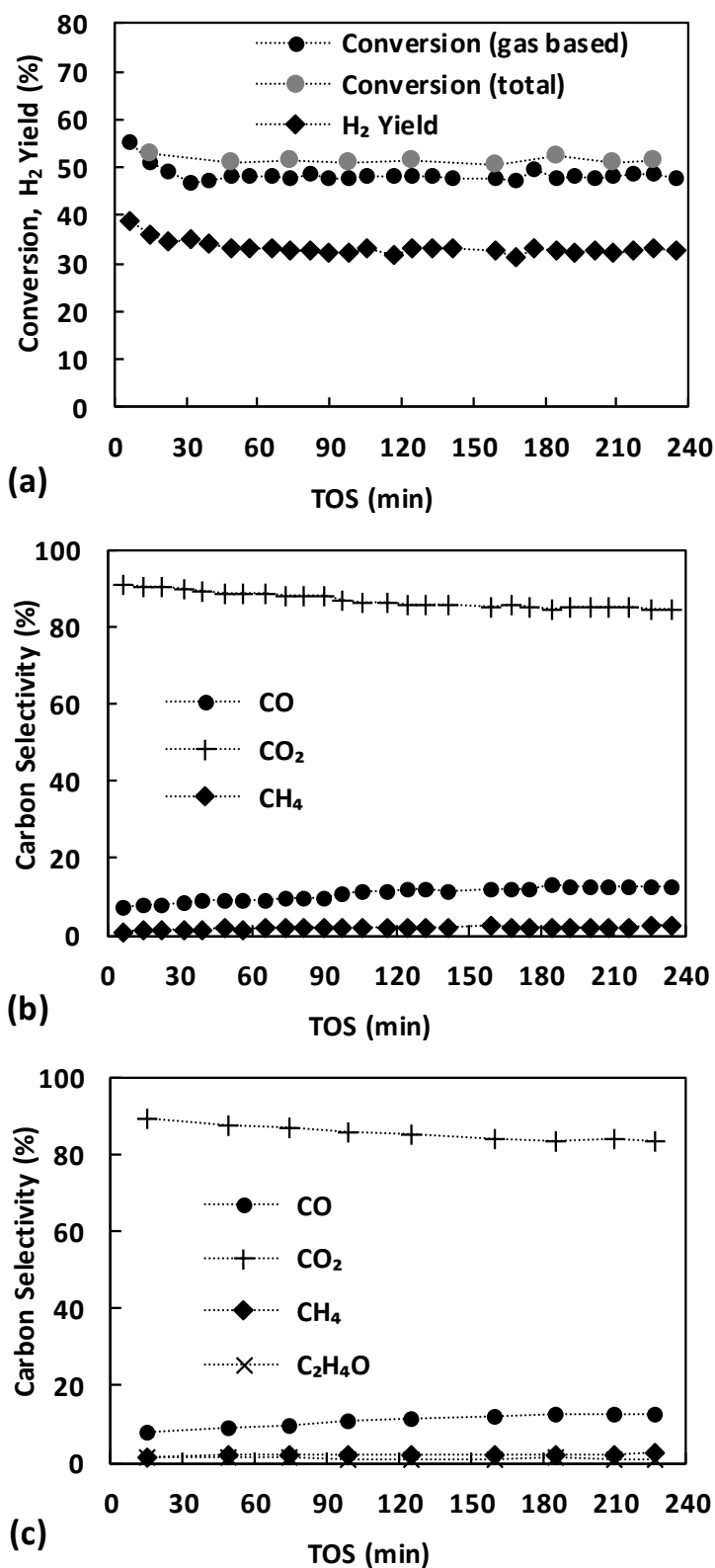


Figure 11. Gas products-based and total ethanol conversion (a), gas products-based carbon selectivities (b) and total carbon selectivities (c) against time-on-stream at 500°C ($W/F_{\text{Eth,tO}} = 358.57 \text{ g}_{\text{cat}} \text{ s g}_{\text{Eth}}^{-1}$, $S/C = 3$).

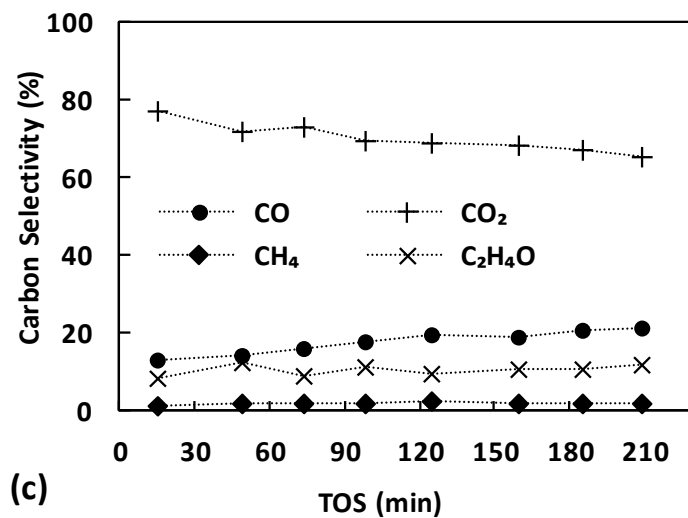
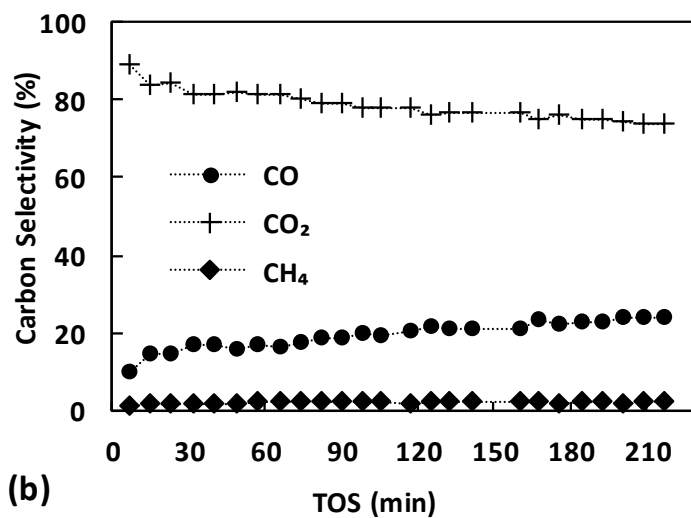
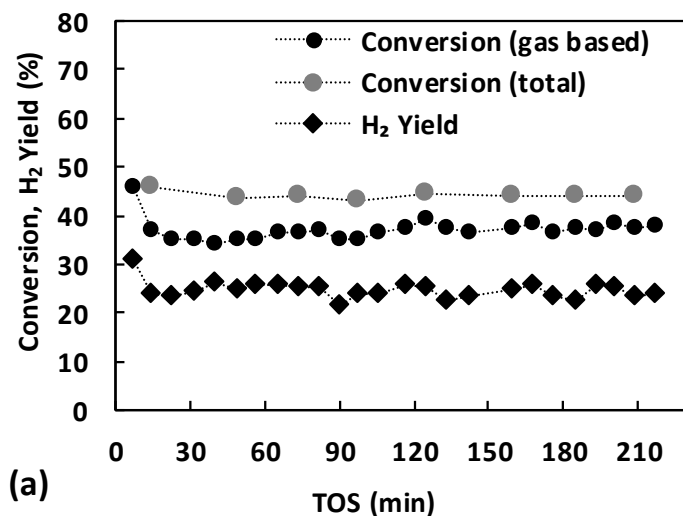


Figure 12. Gas products-based and total ethanol conversion (a), gas products-based carbon selectivities (b) and total carbon selectivities (c) of the regenerated catalyst against time-on-stream at 500°C ($W/F_{\text{Eth},t0} = 358.57 \text{ g}_{\text{cat}} \text{ s g}_{\text{Eth}}^{-1}$, $S/C = 3$).

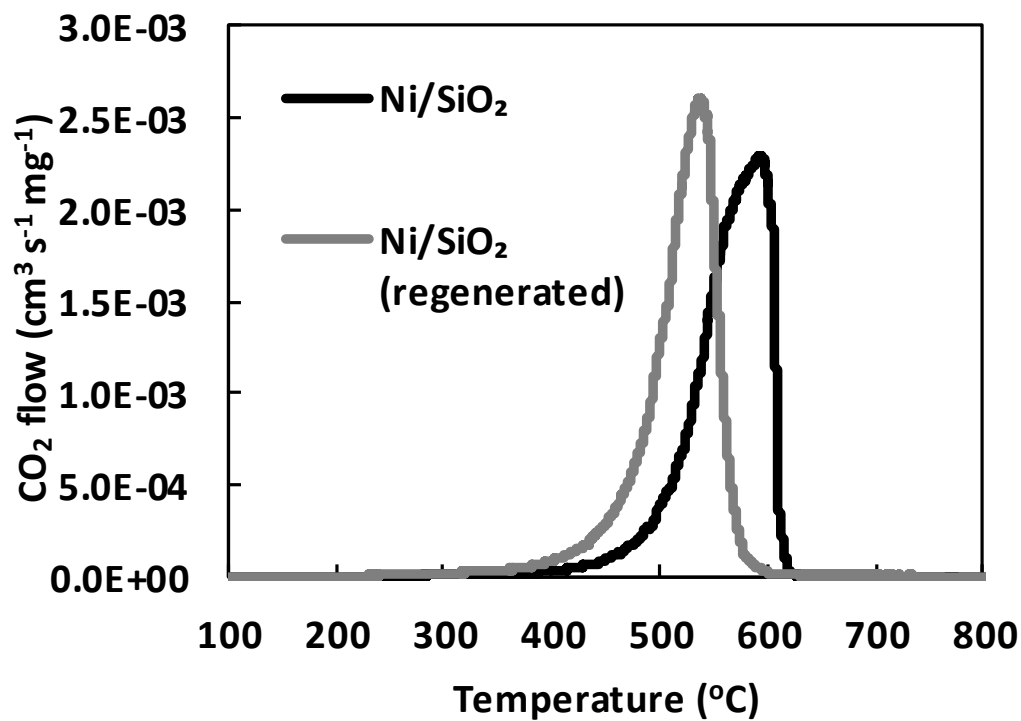


Figure 13. TPO profiles of spent Ni/SiO₂ samples collected after 4 h time-on-stream experiments of ethanol steam reforming at 500°C and S/C = 3 with fresh and regenerated catalysts as described in Section 3.4. Signals normalised per unit mass of catalyst.

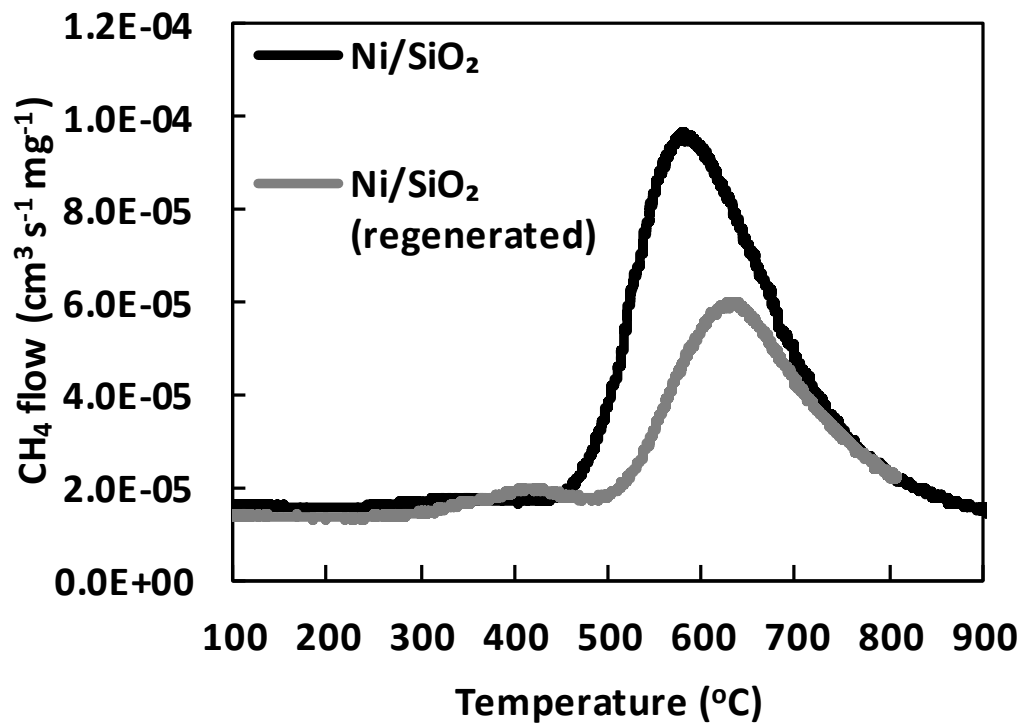


Figure 14. TPH profiles of spent Ni/SiO₂ samples collected after 4 h time-on-stream experiments of ethanol steam reforming at 500°C and S/C = 3 with fresh and regenerated catalysts as described in Section 3.4. Signals normalised per unit mass of catalyst.

A kinetic analysis for the elucidation of metal dominated reaction pathways of the steam reforming of ethanol over Ni

